PHYSICAL REVIEW B VOLUME 26, NUMBER 6 15 SEPTEMBER 1982

New approach for solving the density-functional self-consistent-field problem

Paul Bendt and Alex Zunger
Solar Energy Research Institute, Golden, Colorado 80401
and Department of Physics, University of Colorado, Boulder, Colorado 80309
(Received 26 April 1982)

A new approach for obtaining the minimum of the density-functional total energy is developed by the application of the variational method to the effective potential rather than to wave functions. The resulting conditions on the effective potential are shown to reduce to a system of simultaneous nonlinear equations. This system can then be solved easily with the use of modern ideas from optimization theory. This also gives a unified description of most self-consistency convergence accelerators and enables us to design a superior procedure. The new approach has been implemented in a completely general band-structure method. A special construction of the potential and mixed basis set enables us to calculate efficiently the band structure of materials with both complex unit cells and interacting *d* states. The method is demonstrated on crystalline Si and ZnS and is used to obtain the first *ab initio* band structure for $CuInSe_2$ (8 atoms per unit and 292 electrons per unit cell).

I. INTRODUCTION

The density-functional formalism of Hohenberg, Kohn, and Sham[1,2] (HKS) underlies much of the recent progress in understanding the electronic and structural properties of molecules and solids. HKS have shown that the ground-state charge density and total energy $E_{\rm tot}$ of electrons moving in any given external potential $V_{\rm ext}(\vec{r})$ can be obtained from the expression

$$E_{\rm tot}[n,V_{\rm ext}]=T[n]+\int d\vec{r}\,V_{\rm ext}(\vec{r})n(\vec{r}) +\frac{1}{2}\int d\vec{r}\int d\vec{r}\,'\frac{n(\vec{r})n(\vec{r}\,')}{|\vec{r}-\vec{r}\,'|} +E_{\rm xc}[n] \quad (1)$$

by finding the density $n^*(\vec{r})$ that minimizes $E_{\rm tot}$. (Throughout the paper the asterisk denotes self-consistent ground state.) This form is motivated by the independent-particle model: The first three terms represent, respectively, the kinetic energy, applied potential energy, and classical mean-field interelectronic Coulomb energy of the independent particles. The universal functional $E_{\rm xc}[n]$ represents all corrections to the independent-particle model; i.e., the nonclassical many-body effects of exchange and correlation (xc).

Whereas Eq. (1) is easily proven formally, the evaluation of $n^*[V_{\rm ext}]$ can be difficult in practice. The major problems are the following: (i) The functional $E_{\rm xc}[n]$ is at present known only for a few simple systems and must in general be approximated, (ii) the only known prescription for calculating $T[n]$ given only $n(\vec{r})$ (no wave functions) is often insufficiently accurate on the scale of binding energies or conformational energies of polyatomic system,[3] and (iii) current searching algorithms to find $n^*(\vec{r})$ that minimizes $E_{\rm tot}$ are not effective for general polyatomic systems. The first problem is circumvented by applying the local-density approximation for $E_{\rm xc}[n]$; it is determined by borrowing the known solution for the homogeneous electron gas.[2] For the second difficulty, Kohn and Sham proposed bypassing the evaluation of $T[n]$ by simultaneously constructing a density $n(\vec{r})$ and its kinetic energy $T[n]$ from a set of wave functions of noninteracting particles. A recent theorem by Theophilou[4] described below shows that these fictitious noninteracting particles form a rigorous foundation for the independent-particle model.

The results of Theophilou have motivated us to find a new approach to solving the density-functional problem. In its final form our approach is quite similar to that of HKS, but it also provides an understanding for the common basis of several computational techniques currently in use. This understanding in turn suggests new techniques for obtaining the solution to the density-functional problem for polyatomic systems. These techniques have been implemented in this paper and result in a very effective procedure for finding the variational self-consistent-field (SCF) potential.

Theophilou[4] (see also Refs. 5 and 6) has shown that for any physical charge density $n(\vec{r})$ there exists a potential $U_{\text{ext}}(\vec{r})$(an ordinary function of $\vec{r}$) in which the noninteracting particles will have the charge density $n(\vec{r})$. The Schrödinger equation for the noninteracting particles is

$$[-\tfrac{1}{2}\nabla^2+U_{\text{ext}}(\vec{r})]\psi_j(\vec{r})=\epsilon_j\psi_j(\vec{r}) . \quad (2)$$

By construction, the charge density of the real system is identical to the charge density of the system of fictitious noninteracting particles given by

$$n(\vec{r})=\sum_j \omega_j |\psi_j(\vec{r})|^2 , \quad (3)$$

where ω_j are occupation numbers. The ground-state kinetic energy in the independent-particle approximation is likewise constructed from the noninteracting particle orbitals as

$$T[n,(\vec{r})]=\sum_j \omega_j \langle \psi_j(\vec{r}) | -\tfrac{1}{2}\nabla^2 | \psi_j(\vec{r})\rangle . \quad (4)$$

Theophilou proved a one-to-one-to-one correspondence among the generating potential $U_{\text{ext}}(\vec{r})$ (up to an additive constant), the ground-state charge density $n(\vec{r})$, and the ground-state orbitals $\{\psi_j(\vec{r})\}$ for the noninteracting particles (and a similar correspondence also for real electrons). Notice that $U_{\text{ext}}(\vec{r})$ contains the information of the fixed external potential $V_{\text{ext}}(\vec{r})$ [Eq. (1)] which, together with the number of electrons $N=\sum_j \omega_j$, defines the physical system. Notice further that the only meaning for $U_{\text{ext}}(\vec{r})$ is that it generates the charge density and kinetic energy via Eqs. (2)—(4).

In the density functional equation (1), the density $n(\vec{r})$ is formally the independent variable. However, given an $n(\vec{r})$, it is difficult to find the corresponding $T[n]$ (unless approximate gradient series expressions[3] are used for $T[n]$). Theophilou's theorem, however, opens the way to treating either the orbitals $\{\psi_j(\vec{r})\}$ (as done by HKS and almost all subsequent applications of the density-functional formalism) or the generating potential $U_{\text{ext}}(\vec{r})$ (as done here) as the independent variable for minimizing the total energy in Eq. (1). While these two approaches are parallel, they still represent fundamentally different philosophical viewpoints, which in turn are translated into different computational schemes. As shown below, the scheme based on regarding $U_{\text{ext}}(\vec{r})$ as the independent variable can be adapted to use modern and powerful minimization techniques, which greatly simplifies the solution of the density-functional problem.

We will define the potential variation which is used here by first comparing it to other variational approaches. The choice between the two possible independent variables and the type of variation used leads to four fundamentally different approaches to minimizing the HKS total energy. In practice the minimization is always restricted to searching a finite-dimensional subspace from the total Hilbert space of wave functions or potentials. We will denote the independent variables as functions of both position and a set of variational parameters which specify a point in the given parameter subspace:

$$\psi_j(\vec{r})=\psi_j(\vec{r};\{a_{ij}\}) , \quad (5)$$

$$U_{\text{ext}}(\vec{r})=U_{\text{ext}}(\vec{r};\{\mu_p\}) . \quad (6)$$

Here $\{a_{ij}\}$ and $\{\mu_p\}$ may be either linear or nonlinear parameters. The four approaches to the energy-minimization problem are the following: (i) *wave-function sampling*, i.e., a discrete minimization of $E_{\text{tot}}[n\{a_{ij}\};V_{\text{ext}}]$ by sampling points $\{a_{ij}\}$ and choosing the lowest E_{tot}, (ii) *the wave-function gradient method*, i.e., the Kohn-Sham approach in which one solves the eigenvalue equations resulting from the condition $\nabla_{\vec{a}}E_{\text{tot}}=0$, (iii) *potential sampling*, i.e., a discrete minimization of $E_{\text{tot}}[n\{\mu_p\};V_{\text{ext}}]$ by sampling $\{\mu_p\}$, and (iv) *the potential-gradient method*, i.e., solving the equations resulting from the condition $\nabla_{\vec{\mu}}E_{\text{tot}}=0$.

All but the last approach have been used previously, either in the context of the density-functional energy expression of Eq. (1) or in conjunction with other energy functionals. In the next section we discuss the extent to which these different approaches lend themselves to effective computational schemes. We will show that the potential-gradient method (iv) has important advantages. Section III shows how these advantages can be used to simplify the solution of the noninteracting single-particle equation [Eq. (2)] for solids. Our completely general potential-variation mixed basis method introduced in this section can treat materials with both low symmetry and interacting d bands. In Sec. IV we give an overview of Broyden's method, a powerful optimization method particularly well suited for solving the potential-variation energy-minimization problem. This method requires only quantities already calculated for other purposes but cleverly combines them with the iteration history to find the SCF potential quickly. The illustrative applications of Sec. V show our results for three very different semiconductors: covalently bonded Si, ionic ZnS

with d electrons, and the structurally complex ternary semiconductor $CuInSe_2$.

II. FOUR VIEWS ON THE TOTAL-ENERGY-MINIMIZATION PROBLEM

A. The wave-function sampling method

In this approach one must (i) select a trial parameter set $\{a_{ij}\}$ for Eq. (5) and construct the wave functions $\psi_j(\vec{r};\{a_{ij}\})$ of Eq. (5); (ii) construct the density $n(\vec{r})$ and kinetic energy $T[n]$ from Eqs. (3) and (4), respectively, and (iii) calculate $E_{\rm tot}[n,V_{\rm ext}]$ of Eq. (1) and repeat the above steps to obtain the minimum of $E_{\rm tot}[n\{a_{ij}\};V_{\rm ext}]$ as a function of $\{a_{ij}\}$.

The primary advantage of this method is that it does not require any eigenvalue problem solving, such as Eq. (2), and does not require that any effective potential be constructed. Hence, it is possible to deal conveniently with nonlinear parameters and interelectronic correlation effects directly in the wave functions. Consequently, this method has been used extensively to calculate many-body interaction energies for bosons,[7] nuclear matter,[8] Fermi liquids,[9] solids,[10] and molecules[11] with the use of nonlinear forms such as the Jastrow wave functions[12] $\psi_j(\vec{r}_{12};\{a_{ij}\})$ or Feenberg wave functions[7] $\psi_j(\vec{r}_{12},\vec{r}_{123},\ldots;\{a_{ij}\})$. It has also been used to define Wannier functions for solids.[13] However, for our purpose here of treating systems with a large number of occupied single-particle orbitals $\{\psi_j\}$, this method is very ineffective because it requires a good search method to converge at all and since the number of its variational parameters depends on the number of occupied orbitals. It is therefore limited, with the use of state-of-the-art nonstochastic search algorithms, to about 100 parameters a_{ij}. The result is that this method is suitable for independent-particle problems only when the number of occupied states is small (as simultaneous minimization is required for all single-particle orbitals ψ_j) or when the wave functions have a particularly simple form. Many problems in contemporary one-electron solid-state physics do not satisfy these conditions.

B. The wave-function gradient, or the HKS method

Since the form of the energy-minimizing potential $U_{\rm ext}(\vec{r})$ of Eq. (2) is generally unknown, Kohn and Sham[2] have provided a particular interpretation to it, based on a wave-function variational principle $\partial E_{\rm tot}/\partial\psi=0$. This leads to the condition for the gradient:

$$\frac{\partial E_{\rm tot}}{\partial a_{ij}}=2{\rm Re}\left[\left\langle\frac{\partial\psi_j^*}{\partial a_{ij}}\right|-\frac{1}{2}\nabla^2+V_{\rm KS}[n(\vec{r})]-\epsilon_j\left|\psi_j^*\right\rangle\right]=0\,, \tag{7a}$$

to be satisfied by the final SCF wave functions $\psi^*(r)$. This is more commonly identified as the Kohn-Sham (KS) single-particle equation for the variational wave functions of the fictitious noninteracting particles:

$$[-\tfrac{1}{2}\nabla^2+V_{\rm KS}[n(\vec{r})]]\psi_j^*(\vec{r})=\epsilon_j\psi_j^*(\vec{r})\,. \tag{7b}$$

This is identical in form to the general Eq. (2) that generates orbitals $\{\psi_j\}$, except that $U_{\rm ext}(\vec{r})$ of Eq. (2), which is an ordinary function of $\vec{r}$, is replaced in Eq. (7b) by an integrodifferential operator,

$$V_{\rm KS}[n(\vec{r})]\equiv V_{\rm ext}(\vec{r})+\int dr\frac{n(\vec{r}\,')}{|\vec{r}-\vec{r}\,'|}+\frac{\partial E_{\rm xc}[n]}{\partial n(\vec{r})}\equiv V_{\rm ext}(\vec{r})+V_{\rm Coul}[n,(\vec{r})]+V_{\rm xc}[n(\vec{r})]\,, \tag{8}$$

where $V_{\rm Coul}[n(\vec{r})]$ and $V_{\rm xc}[n(\vec{r})]$ are the interelectron Coulomb and xc potentials, respectively. The explicit dependence of the Kohn-Sham potential on the charge density requires that the variational Eqs. (7) and (8) be solved iteratively. The general description of this iterative procedure is as follows: (i) Select a trial set $\{a_{ij}\}$ and construct the wave functions $\{\psi_j(\vec{r}_j;\{a_{ij}\})\}$ of Eq. (5); (ii) construct the charge density $n(\vec{r})$ and kinetic energy $T[n]$ using Eqs. (3) and (4); (iii) from the charge density calculate the Kohn-Sham potential $V_{\rm KS}[n,(\vec{r})]$ of Eq. (8); (iv) solve the eigenvalue problem [Eq. (7)] to obtain new wave functions. Repeat all of the above steps until the input and output wave functions are equal (to within a prescribed tolerance).

This method has an important advantage over the wave-function sampling method: At an arbitrary mth iteration it yields solutions for a set of wave functions $\{\psi_j^{(m)}(\vec{r})\}$ which contain substantially more information than the single number $E_{\rm tot}^{(m)}$ provided by the wave-function sampling method. This information then can be used as a guide for selecting the next trial wave functions.

This procedure has been implemented in the past

with various computational approximations, including (i) the size and form of the basis set describing $\{\psi_j\}$, (ii) the calculation of $V_{\rm KS}[n(\vec{r})]$ from $n(\vec{r})$, (iii) the solution of the eigenvalue problem in Eq. (7), and (iv) the specification of a consistency between input and output wave functions. However, a number of annoying features remain. These include the high sensitivity of $n(\vec{r})$ to computational fluctuations in $V_{\rm KS}(\vec{r})$ (which often leads to instabilities in iterative schemes, e.g., Ref. 14) and the large size of the subspace $\{a_{ij}\}$ needed to obtain a useful accuracy.[15] These difficulties frequently lead to the introduction of (often severe) computational approximations to solve the all-electron Kohn-Sham problem. In part they also encourage a pseudopotential approach to the problem[16] in which $V_{\rm KS}(\vec{r})$ in Eq. (8) is replaced by an approximate functional identifying $V_{\rm ext}(\vec{r})$ with an empirical pseudopotential and treating only the valence electrons.

The method for selecting trial wave functions $\psi_j^{(m)}(\vec{r})$ for the mth iteration implied by the Kohn-Sham approach is simply $\psi_j^{(m)}(\vec{r})=\tilde{\psi}_j^{(m-1)}(\vec{r})$, where $\tilde{\psi}_j^{(m-1)}(\vec{r})$ is the solution of Eq. (7) for the previous $(m-1)$ iteration. Although obvious and simple, this leads to an iteration sequence which is not guaranteed to converge and often does not, as will be illustrated in Sec. V for ZnS. In attempts to overcome this problem, as well as those indicated above, various artificial devices for forcing convergence have been used. These include the potential-mixing method (e.g., Ref. 16), the Pratt scheme,[17] improved mixing schemes,[18] or potential-attenuation schemes.[19] These methods all modify the potential of Eq. (8) by including contributions from previous iterations in various manners. Although these have yielded solutions for many interesting systems, the convergence is generally slow and the inherent instabilities in such methods remain formidable. Furthermore, in the context of the Kohn-sham variational scheme *such methods are formally illegitimate:* Given a charge density $n^{(m)}(\vec{r})$ for some iteration m, the potential is formally determined by Eq. (8) alone. The potential-gradient method introduced in Sec. II D below, in its treatment of $U_{\rm ext}(\vec{r})$ rather than $\{\psi_j(\vec{r})\}$ as the independent variable, provides both an explanation for frequent failure of *ad hoc* convergence accelerators in the context of the Kohn-Sham approach and a formalism in which a rapidly convergent method is easily found.

C. The potential-sampling method

The potential-sampling method focuses on the original wave-function-generating potential of Eq. (2) rather than on the Kohn-Sham interpretation of it [Eq. (8)]. In this approach one (i) selects a trial set $\{\mu_p\}$ in Eq. (6) and constructs the generating potential $U_{\rm ext}(\vec{r};\{\mu_p\})$ [Eq. (6)] from it; (ii) solves the independent-particle equation [Eq. (2)] to get the wave functions $\{\psi_j(\vec{r})\}$; (iii) constructs the density $n(\vec{r})$ and kinetic energy $T[n]$ from Eqs. (3) and (4), respectively; and (iv) calculates $E_{\rm tot}[n(\mu_p);V_{\rm ext}]$ and repeats the above steps to minimize the energy with respect to $\{\mu_p\}$. In this approach $U_{\rm ext}(\vec{r};\{\mu_p\})$ is only used to generate wave functions whereas the physical potential $V_{\rm ext}(\vec{r})$ is used to evaluate the total energy.

The primary advantages of this method are its conceptual simplicity and the ease of getting crude solutions to simple (e.g., one-dimensional) problems. Much like the wave-function sampling method, it does not require the calculation of the complicated $V_{\rm KS}[n(\vec{r})]$ but rather that of the far simpler generating potential $U_{\rm ext}(\vec{r};\{\mu_p\})$. However, as is true for any sampling method, the potential-sampling approach also has the serious drawback in that it provides at each iteration only the single number $E_{\rm tot}^{(m)}$. Its low informational content makes it difficult to construct an effective trial potential for the subsequent iterations. Furthermore, because the convergence of the sampling becomes dramatically more difficult as the number of variables $\{\mu_p\}$ increases, in most applications only a small number of parameters were used (e.g., two in Ref. 19). With so little variational freedom in the potential, the results are not particularly accurate relative to those obtained by the Kohn-Sham wave-function-gradient method.[20] This method was applied recently in the density-functional context to the problem of the jellium surface[20] and electron-hole drops,[21] and in the context of Thomas-Fermi and Hartree-Fock energy functionals to the calculation of the energies of isolated ions.[22,23] No applications have been reported on the electronic structure of real solids.

D. The potential-gradient method

All of the advantages of the wave-function-gradient method and the potential-sampling method can be combined in the potential-gradient method. In this approach one solves the equations resulting from zeroing the *analytic* gradient of the total energy [Eq. (1)] with respect to the potential variational parameters $\{\mu_p\}$

[Eq. (6)]. In Appendix A we show that this condition results in

$$\frac{\partial E_{\rm tot}}{\partial \mu_p}=0=2\,\mathrm{Re}\left\{\sum_j\sum_{j'\neq j}\omega_j\frac{1}{\epsilon_{j'}-\epsilon_j}\langle\psi_j^*(\vec{r})\,|\,V_{\rm KS}-U_{\rm ext}\,|\,\psi_{j'}^*(\vec{r})\rangle\left\langle\psi_{j'}^*(\vec{r})\left|\frac{\partial U_{\rm ext}}{\partial\mu_p}\right|\psi_j^*(\vec{r})\right\rangle\right\}, \tag{9}$$

where $V_{\rm KS}$ is given by Eq. (8) and $U_{\rm ext}$ is an *ordinary local function of* $\vec{r}$, by Eq. (6). This is the fundamental equation in our approach, and is variationally equivalent to the Kohn-Sham condition in Eq. (7). To satisfy this condition, it is sufficient to have

$$V_{\rm KS}(\vec{r})-U_{\rm ext}(\vec{r};\{\mu_p\})=0\,, \tag{10}$$

which causes the first matrix element in every term in Eq. (9) to vanish.

The steps involved in this approach are as follows: (i) Select a trial set $\{\mu_p\}$ and construct from it the potential $U_{\rm ext}(\vec{r};\{\mu_p\})$ of Eq. (6); (ii) solve the independent-particle eigenvalue equation [Eq. (2)] to obtain $\{\psi_j(\vec{r})\}$ and $\{\epsilon_j\}$; (iii) construct the charge density $n(\vec{r})$ from the orbitals $\{\psi_j(\vec{r})\}$ [Eq. (3)]; (iv) from $n(\vec{r})$ construct $V_{\rm KS}[n(\vec{r})]$ of Eq. (8) and repeat the above steps until $V_{\rm KS}[n(\vec{r};\{\mu_p\})]=U_{\rm ext}(\vec{r};\{\mu_p\})$.

The main advantage of this method over the potential-sampling technique is that each iteration yields the function $V_{\rm KS}^{(m)}(r)-U_{\rm ext}^{(m)}(r)$ rather than the single number $E_{\rm tot}^{(m)}$. This provides much more information on which to base the next trial potential $U_{\rm ext}^{(m+1)}(\vec{r})$. Thus fewer "wrong guesses" are needed before finding the unique self-consistent potential. At the same time, one can include enough free parameters in the potential to obtain accurate results. The advantage of potential gradients over the Kohn-Sham approach is the ease of incorporating and understanding sophisticated strategies for selecting trial potentials. Although the major steps described are the same as for the Kohn-Sham method, there is no implication that the potential used for the eigenvalue problem [Eq. (2)] should be $V_{\rm KS}(\vec{r})$ or any *ad hoc* manipulation of it. Thus the construction of the potential for the single-particle problem is no longer viewed as an *ad hoc* procedure or as a convergence accelerator; instead it is viewed as a particular *searching* procedure. The great advantage of this point of view is that one can apply to it modern general search methods which have been developed in numerical optimization theory. Some of these methods will reach the desired potential with much fewer wrong guesses than any SCF convergence accelerators so far described in the literature.

At the minimum of the total energy, Eq. (10) must be satisfied, implying that at the solution μ^*, the output potential $V_{\rm KS}(\vec{r})$ can be written in the same analytic form as $U_{\rm ext}(\vec{r})$. We assume this is also true for some domain around μ^*; i.e., that there exist some $\{\nu_q\}$ such that

$$V_{\rm KS}[\vec{r};\{\mu_p\}]=U_{\rm ext}[\vec{r};\{\nu_q(\mu_p)\}]\,, \tag{11}$$

where the values for ν are obtained deterministically from the input potential parameters. Equation (10) can then be satisfied by requiring

$$\nu_q(\mu_p^*)=\mu_q^*\,, \tag{12}$$

at the solution μ^*. Arranging the values for μ and ν as column vectors we can define the vector function

$$\vec{\rm F}(\vec{\mu})=\vec{\nu}(\vec{\mu})-\vec{\mu}\,. \tag{13}$$

The condition for minimization of the total energy then becomes

$$\vec{\rm F}(\vec{\mu}^*)=\vec{0}\,. \tag{14}$$

Thus obtaining self-consistency is reduced to finding the zero of this vector function or, equivalently, solving a system of simultaneous nonlinear equations. This can be done very efficiently with the powerful quasi-Newtonian techniques, well known in optimization theory.[24] This method is much less prone to diverge than the Kohn-Sham wave-function-gradient method, and it also provides insight into the successes and failures of various *ad hoc* iterative procedures used in the latter approach. Before describing the foundations and applications of the quasi-Newtonian method, we describe in the next section our techniques for evaluating $\vec{\rm F}(\vec{\mu})$ given a particular trial potential μ. This is basically a procedure for solving the independent-particle problem.

III. FORMAL TECHNIQUES

A. General form of wave functions and potentials

We have used a mixed basis all-electron method. The mixed basis is used to provide both localized

orbitals for d electrons and a large set of plane waves to ensure adequate variational flexibility. Once localized orbitals have been included, the core states can be treated explicitly with no additional difficulty. No pseudopotential approximations are needed.

We will treat all real-space quantities (potentials, wave functions, and charge densities) in a mixed representation consisting of a multicenter (mc) term and a Fourier series (FS) term. The generic expression is

$$f(\vec{r})=\sum_{\alpha}\sum_{l,m} f_{\alpha lm}(\vec{r}-\vec{\tau}_\alpha)Y_{lm}(\vec{r}-\vec{\tau}_\alpha) + \sum_{\vec{G}} f_G e^{i\vec{G}\cdot\vec{r}} , \quad (15)$$

where τ_α are the atomic sites. This representation makes possible the simultaneous description of the rapidly varying but nearly spherical effects around nuclei and the smooth but nonspherical effects in the bonding region. The two terms are not given comparable degrees of freedom. Since effects near the nuclei do not change much from atoms to crystals, the multicentered term is prefabricated from an SCF atomic solution and kept fixed thereafter. This does not imply any physical approximation since the Fourier-series term is kept completely general. Essentially, we expand in a Fourier series the function which represents the difference between the correct solution and the prefabricated multicentered term.[25] This is always possible provided we include enough Fourier components to converge adequately. In Sec. V we will show that excellent convergence can easily be obtained with only a few Fourier coefficients, with the use of multicentered terms constructed by the following procedure.

The multicentered term on a particular atom α is required to be localized near that atom. In particular, we allow the $f_{\alpha lm}$ to be nonvanishing only in a sphere of prescribed radius $r_{\rm mc}$ around τ_α. Requiring these spheres to be nonintersecting causes all multicenter integrands to vanish identically and greatly simplifies the calculation of matrix elements and charge densities. This forces all interatomic interactions into the Fourier series.

With the use of fast Fourier transforms[26] (FFT), the Fourier-series term can be easily interconverted with values on a regular mesh in the unit cell. A quantity evaluated on such a mesh is referred to as an Fourier-series term in this paper.

B. Potential and basis sets

To describe a crystalline potential, a reasonable first-order approximation is to represent it as a superposition of atomic potentials. We use this approximation only to guide our choice of a variational form for the potential and our selection of basis functions. The problem is constructed so that most of the effort is spent calculating the difference between the crystal and the superposition of atoms. This philosophy[25] suggests a variational form for the potential consistent with our general form in which this difference is expanded in a Fourier series:

$$U_{\rm ext}(\vec{r})\equiv U(\vec{r};\{\mu_p\})=\sum_{\vec{R}_n}\sum_{\alpha} v_\alpha(\vec{r}-\vec{R}_n-\vec{\tau}_\alpha) + \sum_{p}\mu_p e^{i\vec{G}_p\cdot\vec{r}} . \quad (16)$$

Here v_α is the self-consistent-field atomic potential of an appropriate "quasiatom" (see below) α at site $\vec{\tau}_\alpha$, whereas $\vec{R}_n$ are direct-lattice vectors, and $\vec{G}_p$ are reciprocal-lattice vectors. (Although we will write the Fourier series as individual plane waves, in practice stars of plane waves are used so that the potential is constructed to have the symmetry of the crystal space group.) For simple semiconductor crystals we find that the Fourier series converges in 5 to 20 stars as is shown in Sec. V.

The multicentered term for the wave functions is a linear combination of corelike Bloch basis functions constructed from atomic wave functions:

$$\Phi_{\alpha nlm}(\vec{k},\vec{r})=e^{i\vec{k}\cdot\vec{\tau}_\alpha} \times\sum_{\vec{R}_n} e^{i\vec{k}\cdot\vec{R}_n}\frac{P_{\alpha nl}(|\vec{r}-\vec{R}_n-\vec{\tau}_\alpha|)}{|\vec{r}-\vec{R}_n-\vec{\tau}|} \times Y_{lm}(\vec{r}-\vec{R}_n-\tau_\alpha) . \quad (17)$$

In this paper the atomic orbitals which are used for Bloch functions are those for which the isolated atomic wave functions are small outside a radius corresponding to the bond center. (This definition includes transition-metal d orbitals.) We construct a single numerical linear combination of atomic orbitals (LCAO) Bloch function for each atomic core orbital. These functions form part of the basis set, the remainder being plane waves:

$$\Phi_{\vec{G}}(\vec{k},\vec{r})=\frac{1}{\sqrt{\Omega}}\exp[i(\vec{k}+\vec{G})\cdot\vec{r}] . \quad (18)$$

The unit-cell volume is denoted by Ω and all basis functions are normalized over the unit cell.

The atomic solution used for the potential and basis functions is not the traditional isolated atom. We perform two modifications to make the results more suitable for our application—compression and truncation. We have chosen to call the fictitious atoms used for this purpose "quasiatoms."

Compression is done to simulate the effect that in a crystal the electrons of a given atom are confined to a smaller space than in an isolated atom. To mimic this effect, we solve for a self-consistent atom which is squeezed into a Wigner-Sietz (WS) sphere. Conceptually this is similar to renormalized atoms.[27] In practice it is achieved simply by restricting the domain of integration for the Schrödinger and Poisson equations to the Wigner-Sietz sphere with radius $r_{\rm WS}$. Since these are differential equations, boundary conditions must be specified on the sphere. For the Poisson equation we use $v_\alpha(r_{\rm WS})=0$ and for the Schrödinger equation

$$\left[\frac{d}{dr}\frac{P(r)}{r}\right]_{r_{\rm WS}}=0\ . \tag{19}$$

This condition puts a maximum in the valence wave function at $r_{\rm WS}$ and therefore produces bondinglike orbitals. Antibondinglike orbitals with a node at $r_{\rm WS}$ could also be produced by setting $P(r_{\rm WS})=0$.

The atomic potentials and orbitals must be truncated to fit into the nonoverlapping spheres used for the multicentered terms. Any damage done can be corrected for in the Fourier-series parts of the potential and wave functions since the atomic ansatz is only one part of the final crystal solution. For the potential, truncation is achieved by first adding a constant to make $v_\alpha(r_{\rm mc})=0$, and second, by setting $v_\alpha(r\geq r_{\rm mc})=0$. The resulting quasiatom potential is confined to a quasiatom sphere and is continuous. The quasiatom core orbitals are now obtained as the eigenfunctions of this potential. The boundary condition $P(r_{\rm mc})=0$ is used so the basis functions will be continuous through $r_{\rm mc}$.

C. Wave functions and charge density

Once the potential and basis set have been specified, the overlap and Hamiltonian matrix elements are completely determined. Owing to the special form given to our potential and basis set, all overlap, kinetic-energy, and potential matrix elements can be easily computed with no approximations. The simple one-center, one-dimensional expressions used are given in Appendix B. The resulting Hamiltonian and overlap matrices are then diagonalized to obtain wave-function-expansion coefficients.

The method we use for the diagonalization is an iterative eigenvector-search algorithm. The method consists of diagonalizing a small submatrix by Householder transformations and then using high-order (e.g., seventh) perturbation theory to include the remaining elements. The algorithm produces vectors arbitrarily close to the true eigenvectors of the full matrix by continuing the perturbation to a sufficiently high order. This method is much faster than Householder transformations if the number of eigenvectors sought is small compared to the matrix size. The details of this method will be discussed in another paper; for now, it suffices to say that one ultimately obtains true eigenvectors of the full matrix.

The charge density is constructed for a single unit cell ($\vec{\mathbf{R}}_n=0$) and is repeated in each unit cell. The portion of each wave function in the primary unit cell can be written [cf. Eq. (5)] as

$$\begin{aligned}\psi_j(\vec{\mathbf{k}},\vec{\mathbf{r}})&=\sum_i a_{ij}(\vec{\mathbf{k}})\Phi_i(\vec{\mathbf{k}},\vec{\mathbf{r}})\\&=\psi_{{\rm pw},j}(\vec{\mathbf{k}},\vec{\mathbf{r}})+\sum_\alpha \psi_{\alpha j}(\vec{\mathbf{k}},\vec{\mathbf{r}}-\vec{\tau}_\alpha)\ ,\end{aligned} \tag{20}$$

with $\psi_{{\rm pw},j}$ denoting the part from plane-wave basis functions and $\psi_{\alpha j}$ denoting the part from LCAO Bloch functions around atom α. The charge density is then

$$n_j(\vec{\mathbf{k}},\vec{\mathbf{r}})=|\psi_{{\rm pw},j}(\vec{\mathbf{k}},\vec{\mathbf{r}})|^2+\sum_\alpha\{|\psi_{\alpha j}(\vec{\mathbf{k}},\vec{\mathbf{r}}-\vec{\tau}_\alpha)|^2+2\,{\rm Re}[\psi^*_{{\rm pw},j}(\vec{\mathbf{k}},\vec{\mathbf{r}})\psi_{\alpha j}(\vec{\mathbf{k}},\vec{\mathbf{r}}-\vec{\tau}_\alpha)]\}\ . \tag{21}$$

There are no cross terms between different α's, because the LCAO Bloch functions were confined to nonintersecting spheres. The last term can be evaluated in spherical harmonics by first making a spherical harmonic decomposition of $\psi^*_{{\rm pw},j}$ and then using the Clebsch-Gordan coefficient to evaluate the products of Y_{lm}'s. The result becomes

$$n_j(\vec{k},\vec{r})=n_{\mathrm{FS}j}(\vec{k},\vec{r})+\sum_{\alpha}\sum_{l=0}^{l_{\max}}\sum_{m}n_{\alpha lmj}(\vec{k},\vec{r}-\vec{\tau}_\alpha)Y_{lm}(\hat{\vec{r}}-\vec{\tau}_\alpha)\ . \tag{22}$$

Here $l_{\max}$ is treated as a convergence parameter. Most of the contribution to the second term is the spherically symmetrical core charge. In many previous orthogonalized-plane-wave (OPW) calculations (e.g., Ref. 28), only the $l=0$ term was included. The one-state densities $n_j(\vec{k},\vec{r})$ can then be summed with appropriate special $\vec{k}$-point weighting factors to get the total density, which can also be written as having a Fourier-series and a multicenter contribution,

$$n(\vec{r})=\sum_{\vec{k}}\sum_{j}\omega_j(\vec{k})n_j(\vec{k},\vec{r})=n_{\mathrm{pw}}(\vec{r})+\sum_{\alpha}\sum_{l,m}n_{\alpha lm}(\vec{r}-\vec{\tau}_\alpha)Y_{lm}(\vec{r}-\vec{\tau}_\alpha)\ . \tag{23}$$

A specific $\vec{G}$ component of the total charge density is given by

$$n(\vec{G})=n_{\mathrm{FS}}(\vec{G})+\sum_{\alpha}e^{i\vec{G}\cdot\vec{\tau}_\alpha}\frac{4\pi}{\Omega}\sum_{l,m}(-i)^l Y_{lm}(\hat{G})\int_0^{r_m}r^2dr\,j_l(rG)n_{\alpha lm}(r)\ . \tag{24}$$

At this point one may introduce the frozen-core approximation when it is desired. We interpret freezing a core state to mean that the charge density of that core band is approximated by a superposition of the corresponding compressed-atom core-orbital charge densities. This is not a necessary approximation, but it does result in significant computation savings. For those states which are frozen it is not necessary to compute either the wave function or the charge density which are the two most time-consuming operations. The errors introduced by freezing particular core states will be assessed in Sec. V.

D. Output potential

The $\vec{G}$ components of the Coulomb potential are obtained from the charge density as

$$V_{\mathrm{Coul}}(\vec{G})=\frac{4\pi}{|\vec{G}|^2}\left[n(\vec{G})-\sum_{\alpha}Z_\alpha e^{i\vec{G}\cdot\tau_\alpha}\right],\qquad G\neq 0\ . \tag{25}$$

The second term comes from the nuclear potential and the whole expression has the opposite sign of the electrostatic potential because it represents the energy per electron (rather than the energy per positive charge).

Since the true exchange-correlation energy functional is not known, we use the local-density approximation to it. This potential is still difficult to use because it is nonlinear in the charge density. However, the following procedure is suitable because the potential depends only on the local density. Unless otherwise specified, all results are from the use of the Kohn-Sham[3] exchange ($\alpha=\frac{2}{3}$) and a fit to the Ceperley-Alder[29] correlation potential for the unpolarized homogeneous electron gas.[30] Our procedure generates the full mixed representation xc potential from which specific $\vec{G}$ components can be taken using a formula equivalent to Eq. (24). This method is successful because the quasi-atom spheres are nonintersecting. Thus at each point in space we have only one multicentered density to couple with the Fourier-series term.

The approach used is to write

$$V_{\mathrm{xc}}(\vec{r})=\sum_{\alpha}f_\alpha(\vec{r})+\left\{v_{\mathrm{xc}}[n(\vec{r})]-\sum_{\alpha}f_\alpha(\vec{r})\right\}, \tag{26}$$

where the first term will become the multicentered contribution and the curly-bracketed term will be expanded in a Fourier series. The only requirements on the functions f_α are that they be constructed from a small number of spherical harmonics and that they leave the curly-bracketed term rapidly convergent. The only part of V_{xc} which converges too slowly to be left in the Fourier series is the nearly spherical part around each nucleus (within about 0.8 a.u.). By constructing f_α to contain this piece, the Fourier-series term will be smooth (in fact, nearly zero) throughout this region. In order that this term also be smooth between this region and r_{mc}, we will require that f_α fall off smoothly to zero at r_{mc}. These requirements can be met by defining

$$f_\alpha(\vec{r})=v_{\mathrm{xc}}[n_{s\alpha}(|\vec{r}-\vec{\tau}_\alpha|)C(|\vec{r}-\vec{\tau}_\alpha|)\ , \tag{27}$$

where

$$n_{s\alpha}(r)=\frac{1}{4\pi}\oint d^2\hat{r}\, n(\vec{r}+\vec{\tau}_\alpha)$$
$$=\sum_{\vec{G}} e^{i\vec{G}\cdot\tau_\alpha} n_{\mathrm{FS}}(\vec{G}) j_0(Gr)+\frac{1}{\sqrt{4\pi}} n_{\alpha 00}(r) \tag{28}$$

and

$$C(r)=\begin{cases} 1, & r\le r \\ \frac{1}{2}\left[1+\cos\left[\pi\dfrac{r-r_2}{r_{\mathrm{mc}}-r_1}\right]\right], & r_1\le r\le r_{\mathrm{mc}} \\ 0, & r_{\mathrm{mc}}\le r \end{cases} \tag{29}$$

are the spherically symmetrized density around $\vec{\tau}_\alpha$ and a smooth cutoff function, respectively. (We use $r_1=1.0$ a.u.) Different values will give different f_α, *but must give the same* v_{xc}. Given this definition of f_α, one can now evaluate the second term of Eq. (26) on a regular mesh in real space and use a fast Fourier transform[26] to evaluate it in $\vec{G}$ space. Convergence can be proven with the use of progressively finer real-space meshes until no further improvement is obtained in the $\vec{G}$ components.

One additional point in our method is that the nonspherical density in the multicentered terms is included only to first order. In principle this is justified by the fact that the nonspherical density is small and is in a region where $V_{\mathrm{xc}}[n]$ is relatively flat; that is, a region where the total density (mainly the spherical core density) is large. In practice, this approximation is justified by the fact that even this first-order term is negligibly small. The details of this first-order approximation are given in Appendix B.

After obtaining the Coulomb and xc potentials that make up $V_{\mathrm{KS}}(\vec{r})$, we wish to fit the potential to the form Eq. (11) by obtaining the parameters $\{v_q\}$. Since the Fourier series used in the analytic form is made of a linear combination of orthonormal functions, the best fit (in a least-squares sense) requires simply taking Fourier components. Thus,

$$v_q=V_{\mathrm{Coul}}(\vec{G}_q)+V_{\mathrm{xc}}(\vec{G}_q)-\sum_\alpha v_\alpha(\vec{G}_q)\ , \tag{30}$$

where $v_\alpha(\vec{G})$ are Fourier components of the atomic potentials, given by Eq. (B8).

IV. SEARCHING FOR THE ENERGY MINIMUM

We now have a well-defined procedure for obtaining the output parameters $\{v_q\}$ for an arbitrary set of input parameters $\{\mu_p\}$. The remaining problem is to find the set that minimizes total energy, or equivalently, that set which gives a zero of $\vec{F}(\vec{\mu})$ from Eq. (13). In this section we will describe briefly the quasi-Newtonian method which we use. Of the many available methods, this one is particularly well suited for the self-consistency problem for a number of reasons. First, the method does not require new information; it uses only the quantities needed for the band-structure calculation. Second, the method "remembers" information from all past iterations and is able to use this information effectively in constructing the best guess for $\{\mu_p^{(m)}\}$ for the next iteration. This property results in better guesses (i.e., more rapid convergence) than any method using only the most recent iteration, or the most recent few iterations. In particular, the approach is considerably more effective than potential mixing,[16,17] the convergence accelerator of Ferriera,[18] or the potential attenuation scheme.[19] A third advantage is that this method automatically discounts information from the distant past, so if it is not confused by nonlinearity, as is the subspace inversion method advocated by Puley.[31] The method can be adopted almost to any (molecular or solid-state) electronic structure method. Application to the plane-wave pseudopotential method[16] is trivial and has resulted in exceptionally good SCF convergence even for difficult problems (e.g., surfaces).

In setting up the problem for the quasi-Newtonian method, we must construct the column vectors $\vec{\mu}$ and $\vec{v}$ of Eq. (13). However, the obvious construction of aligning the $\{\mu_p\}$ and $\{v_q\}$ to make complex vectors is not satisfactory since it gives an $\vec{F}(\mu)$ that is not analytic. This arises from the real-part operation in the derivative of $\vec{v}(\vec{\mu})$ [see Eq. (A12)], which is not an analytic operation. This problem can be circumvented by converting the real and imaginary parts of any complex μ_p into two separate components of the real vector $\vec{\mu}$, and similarly for $\vec{v}$. This construction does not affect the definition of $\vec{F}(\vec{\mu})$ from Eq. (13), nor the requirement for minimum energy from Eq. (14). This is essentially equivalent to defining the potential from a real sine-cosine Fourier series rather than from a complex exponential Fourier series, and is a completely legitimate definition for the potential.

Our method to search for zeros of $\vec{F}(\vec{\mu})$ is based on the Newton-Raphson method. This is obtained by writing (for the mth iteration)

$$\vec{F}(\vec{\mu})\approx\vec{F}(\vec{\mu}^{(m)})+\underline{J}^{(m)}[\vec{\mu}-\vec{\mu}^{(m)}]\ . \tag{31}$$

If $\underline{J}^{(m)}$ is the Jacobian matrix $\partial\vec{F}(\vec{\mu}^{(m)})/\partial\vec{\mu}^{(m)}$, then this expression represents the first two terms of the Taylor-series expansion of $\vec{F}(\vec{\mu})$. In practice the Jacobian is hard to compute [(Eqs. (A9) and (A12)], so we use an approximation to it, $\underline{J}^{(m)}$. The procedure for generating $\underline{J}^{(m)}$ will be described shortly. The Newton-Raphson method chooses the $\vec{\mu}^{m+1}$ for the next iteration which will make the right-hand side of Eq. (31) vanish, hoping that this will make the left-hand side very nearly vanish. The right-hand side is made to vanish by setting

$$\vec{\mu}^{(m+1)}=\vec{\mu}^{(m+1)}-[\underline{J}^{(m)}]^{-1}\cdot\vec{F}(\vec{\mu}^{(m)}) . \quad (32)$$

The convergence rate for this procedure depends on how well $\underline{J}^{(m)}$ approximates the true Jacobian. Unfortunately, there is very little information available that sheds light on the structure of the Jacobian. However, for each of the previous iterations, we have $\vec{\mu}^{(m)}$ and its corresponding $\vec{F}(\vec{\mu}^{(m)})$. After a couple of iterations have been accumulated, this "historic" information can be used to provide an acceptable approximation to $\underline{J}^{(m)}$. One technique for incorporating this method which has been found to perform well is Broyden's method.[24] This method requires that $\underline{J}^{(m)}$ satisfy Eq. (31) exactly for the last step made for each iteration (after the first), that is,

$$\vec{F}(\vec{\mu}^{(m-1)})=\vec{F}(\vec{\mu}^{(m)})+\underline{J}^{(m)}[\vec{\mu}^{(m-1)}-\mu^{(m)}] . \quad (33)$$

However, this places only N constraints on the N^2 elements of $\underline{J}^{(m)}$. One can completely specify $\underline{J}^{(m)}$ and simultaneously retain information from further in the past by requiring that $\underline{J}^{(m)}$ be as close as possible to $\underline{J}^{(m-1)}$, while still satisfying Eq. (33). The appropriate definition of "as close as possible" is that the Frobenious norm of the difference be minimized, i.e.,

$$\min\sum_{jk}[J_{jk}^{(m)}-J_{jk}^{(m-1)}]^2 . \quad (34)$$

The constraint of Eq. (33) can be included by Lagrange multipliers, and the minimization is carried out to yield

$$\underline{J}^{(m)}=\underline{J}^{(m-1)}+\frac{[\vec{F}^{(m-1)}-\vec{F}^{(m)}-\underline{J}^{(m-1)}(\vec{\mu}^{(m-1)}-\vec{\mu}^{(m)})](\vec{\mu}^{(m-1)}-\vec{\mu}^{(m)})^t}{|\vec{\mu}^{(m-1)}-\vec{\mu}^{(m)}|^2} . \quad (35)$$

Broyden's method still requires an initial guess for $\underline{J}^{(1)}$ when no information is available. If nothing is known, it is easiest to use a diagonal constant matrix,

$$\underline{J}^{(1)}=-\frac{1}{\alpha}\underline{I} . \quad (36)$$

It is instructive to see what this gives for the second iteration. Combining this with Eqs. (13) and (32) gives

$$\vec{\mu}^{(2)}=\vec{\mu}^{(1)}+\alpha\underline{I}(\vec{\nu}^{(1)}-\vec{\mu}^{(1)})=(1-\alpha)\vec{\mu}^{(1)}+\alpha\vec{\nu}^{(1)} . \quad (37)$$

Since the potential is linear in $\vec{\mu}$, this is simply potential mixing. Thus, approximating $\underline{J}^{(m)}$ by a constant is equivalent to potential mixing (e.g., Ref. 16).

Another procedure for choosing $\underline{J}^{(1)}$ is to recognize that the Jacobian has physical significance. It represents the response of the system in question to a small change in the effective potential. Thus one would expect it to be related to the dielectric susceptibility which is also the response to a small perturbing potential. In fact, it can be shown that the Jacobian, as defined, is the negative of the dielectric kernel. Thus one can use a simple approximation to the dielectric function to obtain a $\underline{J}^{(1)}$. One such model is Thomas-Fermi screening (e.g., Ref. 32), which is diagonal in $\vec{G}$ space. For our $\vec{G}$-space potential this gives a diagonal Jacobian with elements,

$$J_{pp}^{(1)}=-(1+\kappa^2/|\vec{G}_p|^2) , \quad (38)$$

where

$$\kappa=\sqrt{4k_F/\pi} \quad (39)$$

and k_F is the Fermi momentum. It is worth noting that this Jacobian approximation, without updating, is precisely equivalent to the method proposed by Kerker.[19(b)] With updating, it can be expected (cf. Sec. V) to perform much better than he observed. When it is necessary to use a very large number of variational parameters, e.g., more than 200, better efficiency can be achieved by using the complimentary Broyden method discussed in Ref. 24.

V. RESULTS

Our approach to the density-functional problem has been used on a number of systems. Some of the tests performed on it are described in this section. Section V A discusses internal convergence tests to demonstrate that each convergence parameter is being set appropriately. Section V B provides comparisons with recent results of other methods to show the reliability of the present method. One of the principal advantages of the present method is its rapid SCF convergence, which is compared to other techniques in Sec. V C. Finally, Sec. V D gives the first self-consistent band structure available for $CuInSe_2$. This structurally complex semiconductor is of great interest for solar-energy photovoltaic applications.

A. Convergence

Section III, which described the formal techniques, left several sums with unspecified upper bounds, such as sums over Fourier components. These upper limits are treated as convergence parameters. We now demonstrate that good convergence can be achieved without requiring excessive computation time. First we will look at those parameters used within each SCF iteration. The convergence rates are consistent with those found by earlier workers using the OPW method.[28] Second, a new convergence parameter introduced for this method is the number of potential components μ which are used in Broyden's procedure. This convergence parameter is explored carefully and it is found that the number required is quite modest. Then the frozen-core approximation is examined to see which core states can be frozen without seriously affecting the results. All the convergence calculations were performed using Ceperley-Alder[29,30] exchange-correlation expressions. All results are individually iterated to SCF under the conditions specified.

For zinc-blende structure materials we have established a standard set of convergence parameters which give both very good energy bands and charge densities [Eqs. (18) and (20)] with very modest computational effort. These are (i) about 140 plane waves per atom [Eqs. (18) and (20)], (ii) multicentered charge density expanded up to $l=3$ [Eq. (23)], (iii) about 15 mesh points per cubic a.u. for evaluating the xc potential in Eq. (26) (4096 total), (iv) two special $\vec{k}$ points for Brillouin-zone (BZ) averaging in Eq. (23), and (v) 19 stars for the potential variation in Eq. (16) (16 for homopolar compounds).

These cutoff values are varied to show that each is sufficient. The plane-wave convergence for ZnS is shown by Table I (x-ray scattering factors), and in Fig. 1 for the eigenvalues at Γ. The results are

TABLE I. ZnS x-ray scattering amplitudes in electrons per unit cell for basis-set sizes from 32 to 141 plane waves per atom. The same LCAO basis is used for all calculations.

	No. of pw/atom				
Beam	32	56	84	114	141
(111)	28.42	28.44	28.47	28.48	28.48
(200)	13.24	13.16	13.11	13.09	13.08
(220)	31.31	31.42	31.47	31.49	31.50
(311)	22.02	22.07	22.10	22.11	22.11
(222)	11.39	11.32	11.26	11.24	11.23
(400)	26.14	26.22	26.26	26.29	26.29
(331)	18.89	18.93	18.94	18.95	18.95
(420)	9.31	9.35	9.31	9.28	9.26
(422)	23.07	23.07	23.08	23.09	23.10
(333)	16.59	16.60	16.59	16.58	16.58
(511)	16.60	16.61	16.61	16.60	16.60
(440)	20.73	20.72	20.69	20.69	20.69
(531)	14.90	14.91	14.89	14.88	14.88
(442)	6.59	6.65	6.67	6.66	6.65
(600)	6.60	6.66	6.68	6.67	6.66
(620)	18.84	18.84	18.82	18.80	18.80

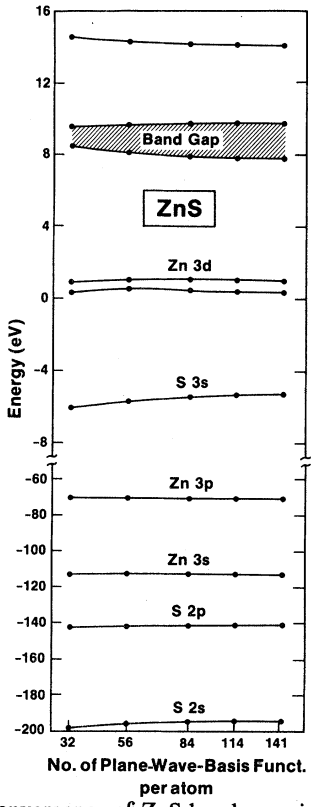

FIG. 1. Convergence of ZnS band energies at Γ vs basis-set size in plane waves per atom.

TABLE II. Silicon band energies in eV and x-ray scattering amplitudes for various convergence parameter setting. For each column, unspecified parameters are set at the standard values as given in the text. The results of a frozen-core approximation (FCA) are given for comparison.

State	Standard	385 pw/atom 51 pt/a.u.^{3} 24 stars	$l=0$	6 $\vec{k}$ points	FCA
$2s$	−132.5	−132.5	−132.5	−132.5	
$2p$	−90.0	−90.0	−90.0	−90.0	
Γ_{1v}	−11.95	−11.96	−11.96	−11.94	−11.94
Γ_{25v}	0.0	0.0	0.0	0.0	0.0
Γ_{15c}	2.50	2.48	2.49	2.51	2.50
Γ_{2c}	3.29	3.26	3.28	3.29	3.28
Γ_{1c}	7.59	7.58	7.59	7.61	7.60
Γ_{12c}	7.88	7.69	7.87	7.89	7.90
X_{1v}	−7.79	−7.80	−7.80	−7.79	−7.78
X_{4v}	−2.90	−2.87	−2.90	−2.89	−2.90
X_{1c}	0.57	0.53	0.57	0.59	0.59
X_{4c}	9.99	9.96	9.99	10.00	9.98
Beam		Scattering amplitudes (electrons per unit cell)			
(111)	15.17	15.28	15.16	15.15	15.15
(220)	17.31	17.31	17.31	17.31	17.27
(311)	11.35	11.35	11.34	11.35	11.31
(222)	0.35	0.35	0.36	0.34	0.35
(400)	14.89	14.88	14.89	14.89	14.84
(331)	10.22	10.21	10.23	10.22	10.17
(422)	13.39	13.38	13.39	13.39	13.34
(332)	9.06	9.05	9.04	9.06	9.01
(511)	9.09	9.08	9.09	9.09	9.04

very stable for any basis larger than 115 plane waves per atom. Even for 55 plane waves per atom the maximum errors are about 0.1 electrons for the scattering factors and 0.3 eV for the band energies. Similar results are found for other $\vec{k}$ points and materials. Convergence was also examined by performing an excessively detailed calculation using 385 plane waves per atom, this time on silicon, as shown in Table II. The only noticeable change is a 0.2-eV drop in the highly sensitive $\Gamma_{12,c}$ state. This calculation also used a large number of potential mesh points (51 points per a.u.^{3}) and stars (24) and shows that the standard settings are converged with respect to these parameters as well. The third column of Table II shows that negligible harm is done by spherically symmetrizing the multicentered charge density, i.e., by including only the $l=0$ term. Since $l=1$ and 2 are forbidden in the zinc-blende structure, one can draw no conclusions regarding their importance. However, the $l=3$ term is demonstrated to be insignificant. The fourth column gives the results of the use of six special $\vec{k}$ points to sample the charge density over the BZ and again no change is seen.

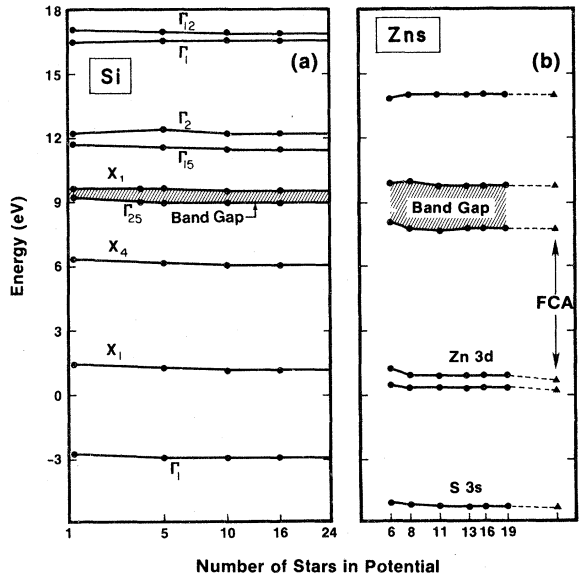

FIG. 2. Convergence of band energies at Γ vs number of stars in Fourier-series potential for (a) silicon and (b) ZnS. The right-hand edge of (b) also gives ZnS energies with the Zn ($1s,2s,2p,3s,3p$) and S ($1s,2s,2p$) core states frozen.

We thus conclude that the standard convergence setting gives more than adequate convergence for zinc-blende structure materials.

The next essential question is whether or not our potential ansatz in Eq. (16) has sufficient variational freedom to reproduce the true SCF potential. To demonstrate this we have explored the convergence of the eigenvalues and charge densities with respect to the number of stars used in the input potential. The eigenvalues results are shown in Fig. 2(a) for silicon and in Fig. 2(b) for ZnS. The Fourier-transform charge of the density are depicted in Table III. As can be seen, even as few as one to five stars give a qualitatively correct picture and beyond about 12 no further improvement can be obtained. We thus conclude that our "standard" setting of 19 stars is more than sufficient.

Finally, we wish to examine the validity of the frozen-core approximation. As stated previously, this approximation is not necessary but does save computer time. In comparing the frozen-core results to the full mixed basis results above, we find the following: The tightly bound core orbitals (i.e., Si $1s$; Zn $1s,2s\,2p$; S $1s$) can be frozen and the matrix elements approximated by Eq. (B9) without affecting any of the results, even in the fifth significant figure. Freezing the next shell (Si $2s,2p$; Zn $3s,3p$; S $2s,2p$) shifts the localized d states by about 0.15 eV but otherwise has little effect. The results in Table II and the right-hand edges of Table III and Fig. 2(b) show that the largest effect on the s and p bands is 0.03 eV and on the x-ray scattering factors is 0.05 electrons. Making the approximation of Eq. (B9) is not appropriate for

TABLE III. X-ray scattering amplitudes for Si and ZnS at self-consistency using different numbers of stars in the Fourier-series potential [Eq. (16)]. The final column for ZnS (FCA) is for 19 stars but with the Zn ($1s,2s,2p,3s,3p$) and S ($1s,2s,2p$) core states frozen. Values are in electrons per unit cell.

			Silicon		
Beam	1 star	5 stars	10 stars	16 stars	24 stars
(111)	15.15	15.16	15.16	15.16	15.16
(220)		17.30	17.29	17.30	17.30
(311)		11.33	11.33	11.34	11.34
(222)		0.37	0.35	0.35	0.35
(400)		14.86	14.87	14.89	14.89
(331)			10.20	10.22	10.22
(422)			13.36	13.39	13.39
(333)			9.03	9.05	9.05
(511)			9.07	9.09	9.09
(440)			12.03	12.06	12.06
(531)				8.20	8.20
(442)				0.02	0.02
(620)				10.91	10.91

			ZnS				
Beam	6 stars	8 stars	11 stars	13 stars	16 stars	19 stars	FCA
(111)	28.45	28.48	28.48	28.48	28.48	28.48	28.48
(200)	13.09	13.12	13.08	13.08	13.08	13.08	13.08
(220)	31.46	31.52	31.50	31.50	31.51	31.51	31.50
(311)	22.06	22.14	22.11	22.11	22.11	22.11	22.10
(222)	11.12	11.25	11.22	11.22	11.23	11.23	11.22
(400)	26.28	26.36	26.30	26.30	26.30	26.30	26.29
(331)		18.99	18.95	18.95	18.95	18.95	18.94
(420)		9.26	9.24	9.25	9.26	9.26	9.24
(422)			23.11	23.10	23.10	23.10	23.09
(333)			16.59	16.58	16.59	16.59	16.57
(511)			16.61	16.60	16.61	16.61	16.59
(440)				20.69	20.69	20.69	20.69
(531)				14.87	14.88	14.88	14.87
(442)					6.65	6.65	6.62
(600)					6.66	6.66	6.63
(620)					18.80	18.80	18.80

these states and leads to eigenvalue errors as large as 1 eV. Similarly, freezing the Zn $3d$ drops this level by about 4 eV and introduces errors in the other bands typically of the order of 1 to 1.5 eV. Thus, we conclude that core states can be frozen without substantial damage, but not transition-metal d states (even in an insulator such as ZnS).

B. Comparisons with previous results

This section is devoted to comparing our results with those of previous calculations. We will compare the silicon results with those of Hamann[33] obtained with the use of the linear augmented-plane-wave method. We will compare our ZnS results with those of Wang and Klein[34] (WK) who have used linear combinations of Gaussian orbitals. Both of these works used the Wigner formula for xc, so for comparison we have done the same for the results shown in Table IV and Fig. 3. Most of the silicon eigenvalues are well within the 0.1-eV error estimated for both methods, the exception being the excited state X_{4c}. For ZnS there are two obvious differences. First, we get the Zn $3d$ states 1.2 eV lower than WK which is undoubtedly due to the difficulty that both methods have in accurately determining highly localized states. Second, we get the conduction band consistently 0.3 to 0.6 eV lower than WK, which we believe to be due to basis set shortcomings in the latter work. (WK use a basis set of only 22 functions per atom as compared to our use of 150.) Too small a basis will raise all the eigenvalues but will raise the conduction bands more than the valence bands. Since WK present no discussion of convergence tests performed, it is impossible to judge the quality of their results.

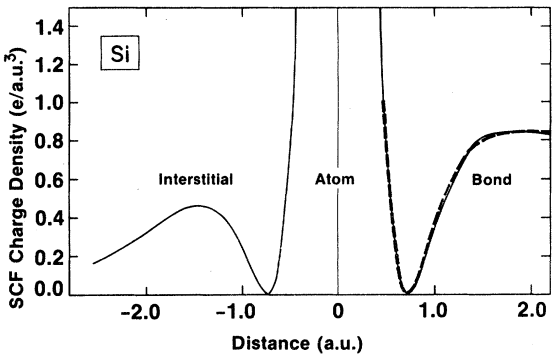

FIG. 3. Silicon charge density from the interstitial region through an atom and to the bond center. Solid line is the present work and dashed is from Ref. 33.

The silicon charge densities, shown in Fig. 3, agree very well with Hamann's results.[33] The only difference is that we get a very slightly ($<1\%$) double-peaked bond which we believe is correct (e.g., it exists also in the excessively detailed calculation). For ZnS all the x-ray scattering factors agree with WK to better than 0.1 electron/unit cell indicating that both methods give substantially the same character for the occupied bands.

TABLE IV. Comparison of the band energies of silicon and ZnS with previous local-density calculations. All results use the Wigner interpolation formula for xc.

Silicon band energies (eV)			ZnS band energies (eV)			ZnS x-ray amplitudes		
State	Present	Ref. 33	State	Present	Ref. 34	Beam	Present	Ref. 34
Γ_{1v}	−11.98	−12.02	Γ_1	−12.93	−12.89	(111)	28.44	28.52
Γ_{25v}	0.0	0.0	Zn $3d$	−7.82	−6.6	(200)	13.01	13.06
				−7.43	−6.2	(220)	31.47	31.54
Γ_{15c}	2.54	2.49	Γ_{15v}	0.0	0.0	(311)	22.07	22.16
Γ_{2c}	3.35	3.18	Γ_{1c}	1.95	2.26	(222)	11.14	11.21
Γ_{1c}	7.48	7.46	Γ_{15c}	6.30	7.04	(400)	26.28	26.35
X_{1v}	−7.79	−7.84	X_{1v}	−11.73	−11.67	(331)	18.93	18.93
X_{4v}	−2.92	−2.82	X_{3v}	−4.81	−4.49	(420)	9.19	9.23
X_{1c}	0.49	0.55	X_{5v}	−2.26	−2.19	(422)	23.12	23.11
X_{4c}	9.99	10.32	X_{1c}	3.14	3.61	(333)	16.60	16.60
L_{2v}	−9.59	−9.64	X_{3c}	4.00	4.58	(511)	16.61	16.61
L_{1v}	−7.04	−7.06	L_{1v}	−12.02	−11.97	(440)	20.74	20.72
L_{3v}	−1.22	−1.16	L_{1v}	−5.38	−5.20			
L_{1c}	1.46	1.40	L_{3v}	−0.89	−0.84			
L_{3c}	3.22	3.77	L_{1c}	3.20	3.65			
			L_{3c}	6.85	7.51			
			L_{1c}	8.52	8.87			

C. Convergence in self-consistency

One of the principal features of our technique is the use of Broyden's powerful update method to lead us efficiently to the SCF potential. Figures 4 and 5 demonstrate the usefulness of this method by comparing convergence rates for different methods. Silicon is not a particularly sensitive test case since it converges well without any special techniques. As shown in Fig. 4, the "no-mixing" results yield acceptable convergence in eight iterations, as do both potential mixing with $\alpha=0.5$ and Thomas-Fermi with $\kappa=1.1$ (obtained from the average valence-band charge density). However, the use of Broyden's method with either of the two later initial Jacobians, significantly improves the convergence rate. Even at iteration 3, the first for which the updates can have an effect, there is a significant improvement. This advantage steadily increases throughout the iteration history. Even for this "easy" case, Broyden's method saves two or three iterations.

For ZnS the improvement shown in Fig. 5 is more dramatic. Both Thomas-Fermi and no-mixing results *diverge* while potential mixing converges slowly, requiring about 14 iterations to reach an acceptable SCF potential. By contrast, with the use of Broyden's method, convergence is reached in seven iterations with either initial $\underline{J}^{(1)}$. Here it is apparent that during the first three or four iterations, the update procedure is contributing little to convergence; however, the Jacobian is "remembering" these iterations and "learning" them. This information is then used in the subsequent iteration to provide rapid convergence.

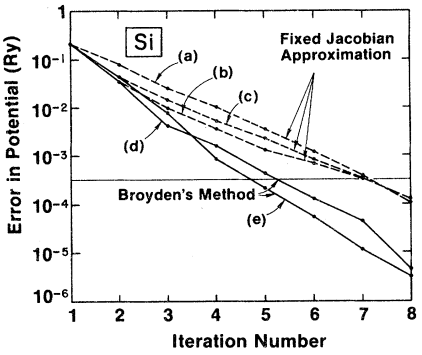

FIG. 4. SCF convergence for silicon. Shown is the logarithm of the largest error in any potential component $|\nu_G-\mu_G|$ vs iteration. Dashed lines are without Broyden's method for (a) no potential mixing; (b) mixing coefficient $\alpha=0.5$; and (c) Thomas-Fermi approximation with $\kappa=1.1$. Solid lines are using Broyden's method starting from (d) potential mixing and from (e) Thomas-Fermi. Horizontal line is our level of acceptable convergence.

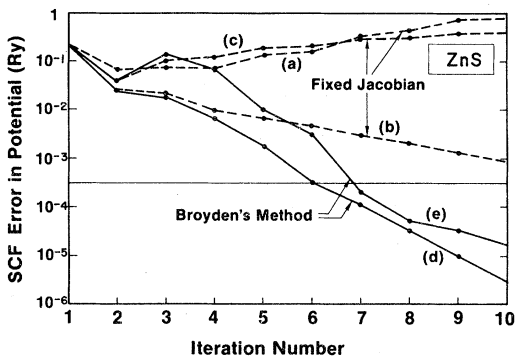

FIG. 5. SCF convergence for ZnS. Cases are the same as in Fig. 4.

In these comparisons, the Thomas-Fermi initial approximations show no advantages over potential mixing. It is expected, however, that for systems with large unit cells the Thomas-Fermi initial guess will be better. For large unit cells, it is the long-wavelength $\vec{G}$ components which oscillate and converge slowly. It is these same spatially slowly varying components which the Thomas-Fermi approximation should treat best.

D. $CuInSe_2$

The previous results show the accuracy and reliability of methods we are using. However, the principal advantage of these methods is the quantum increase in computational power they yield. (They are considerably faster than pseudopotential methods,[16] even though they treat all core states.) This is demonstrated in the present section which presents the results of the first *ab initio* calculation for $CuInSe_2$. This material, and in general the class of ternary chalcopyrites, is of significant technological interest. $CuInSe_2$ is probably the strongest solar-absorbing semiconductor in the solar spectrum. Ternary chalcopyrites are being utilized for solar-energy photovoltaic conversion and are now being subject to extensive experimental research.[35,36] However, in contrast to the zinc-blende compounds, very little theoretical information is available on their electronic properties. The chalcopyrites have a more complicated crystal structure, including eight atoms per unit cell and low point-group symmetry, which makes well-converged electronic structure calculations very

TABLE V. Structural parameters for $CuInSe_2$ and convergence parameter settings for our calculations.

Lattice type and constant	Body centered tetragonal $a=10.93$ a.u. $c=21.86$ a.u.
Primitive lattice vectors	$r_1=(a,0,0)$ $r_2=(0,a,0)$ $r_3=(a/2,a/2,c/2)$
Atomic positions	Cu: $a(0,0,0)$ $a(0,\frac{1}{2},\frac{1}{2})$ In: $a(\frac{1}{2},\frac{1}{2},0)$ $a(\frac{1}{2},0,\frac{1}{2})$ Se: $a(0.224,\frac{1}{4},\frac{1}{4})$ $a(0.776,\frac{3}{4},\frac{1}{4})$ $a(\frac{1}{4},0.724,\frac{3}{4})$ $a(\frac{3}{4},0.276,\frac{3}{4})$
Special $\vec{k}$ points and weights w	
Set of 1	$\frac{2\pi}{a}(\frac{1}{4},\frac{1}{4},\frac{1}{4})$ equivalent to 2 $\vec{k}$ points for ZnS
Set of 18	$\frac{2\pi}{12a}(1,1,1)\omega=1;\frac{2\pi}{12a}(3,3,1)\omega=1$ (1,1,3) 1 (3,3,3) 1 (1,1,5) 1 (3,3,5) 1 (1,3,1) 2 (3,5,1) 2 (1,3,3) 2 (3,5,3) 2 (1,3,5) 2 (3,5,5) 2 (1,5,1) 2 (5,5,1) 1 (1,5,3) 2 (5,5,3) 1 (1,5,5) 2 (5,5,5) 1 equivalent to 28 $\vec{k}$ points for ZnS
Convergence settings	48 pw/atom $l=1$ for charge density 5120 mesh points (4 per a.u.^{3}) 1 special $\vec{k}$ point 40 potential stars
Hamiltonian matrix size	510 basis functions

difficult. The present method is able to overcome the difficulties and we are using it to study these structually complex materials. This paper reports on the results for $CuInSe_2$. Results on the class of I-III-VI_2 chalcopyrites and their chemical trends will be presented in a separate paper.

The structural properties of and convergence parameters used for $CuInSe_2$ are given in Table V. The structure of the unit cell is shown in Fig. 6.

Some of the convergence parameters are not quite as good as for the standard zinc-blende calculations; however, they should be adequate to yield energy eigenvalues within 0.2 eV and x-ray scattering factors within 0.5 electrons per chalcopyrite unit cell. A detailed discussion of the properties of $CuInSe_2$ is outside the scope of this paper and will be postponed to a future publication. We will give here only a brief summary.

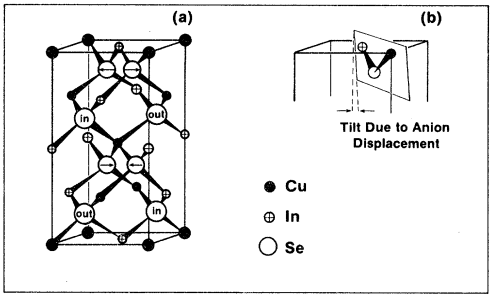

FIG. 6. (a) Structure of the $CuInSe_2$ unit cell. The anion displacement $(\frac{1}{4}-u)$ moves the Se atom in the directions shown by the arrows. (b) Position of the plane for charge-density contours in the same unit cell.

Our results for $CuInSe_2$ are shown in Fig. 7 (density of states), Figs. 8—10 (charge densities), Fig. 11 (band structure), Table VI (band energies), and Table VII (x-ray scattering amplitudes). The total and local densities of states (DOS) are constructed as a histogram of eigenvalues from 18 special $\vec{k}$ points and hence the resolution is rather coarse. The local DOS is the amount of charge within touching spheres of the Pauling radii. This is projected into two components, that orthogonal to the core basis functions, shown by the dashed line, and the remainder which is primarily the outermost d-shell contribution. Our DOS compares well with the x-ray photoelectron spectros-

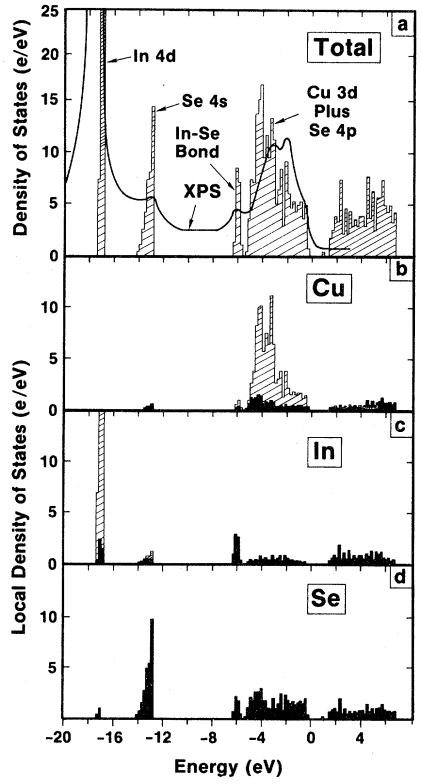

FIG. 7. Densities of states for $CuInSe_2$. (a) Total density of states histogram with XPS results from Ref. 37. Local density of states on (b) Cu, (c) In, and (d) Se. Hatched area represents the total within each atomic mc sphere and the filled area is the amount orthogonal to the corelike basis functions. The difference is roughly the d-state contribution, $3d$ on Cu and $4d$ on In.

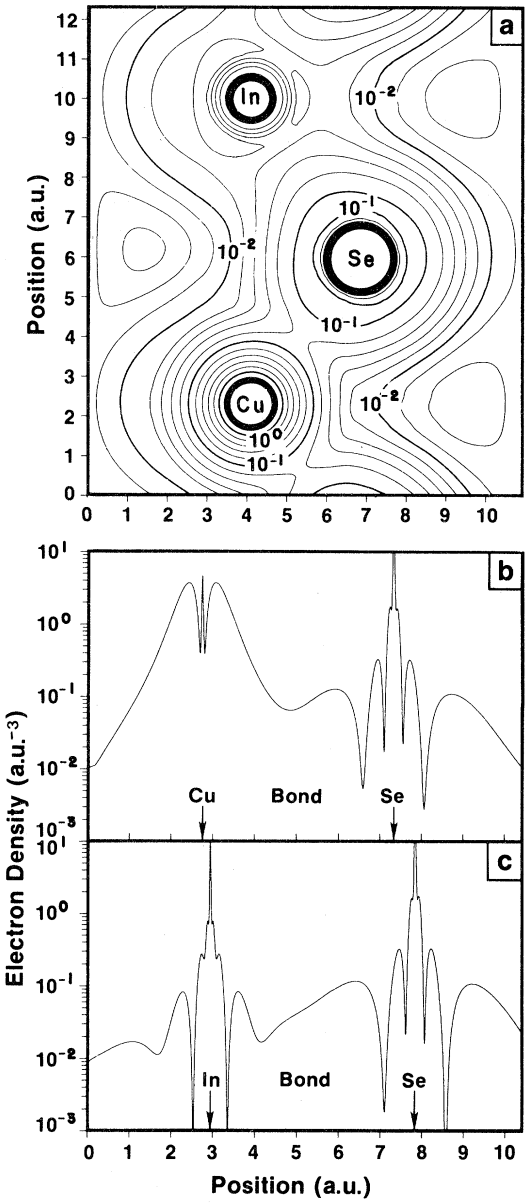

FIG. 8. Valence-band charge density for $CuInSe_2$. Contours (a) are logarithmically spaced; see the text for details. Line plots are through the (b) Cu—Se bond and the (c) In—Se bond. Solid rings in (a) indicate the core regions.

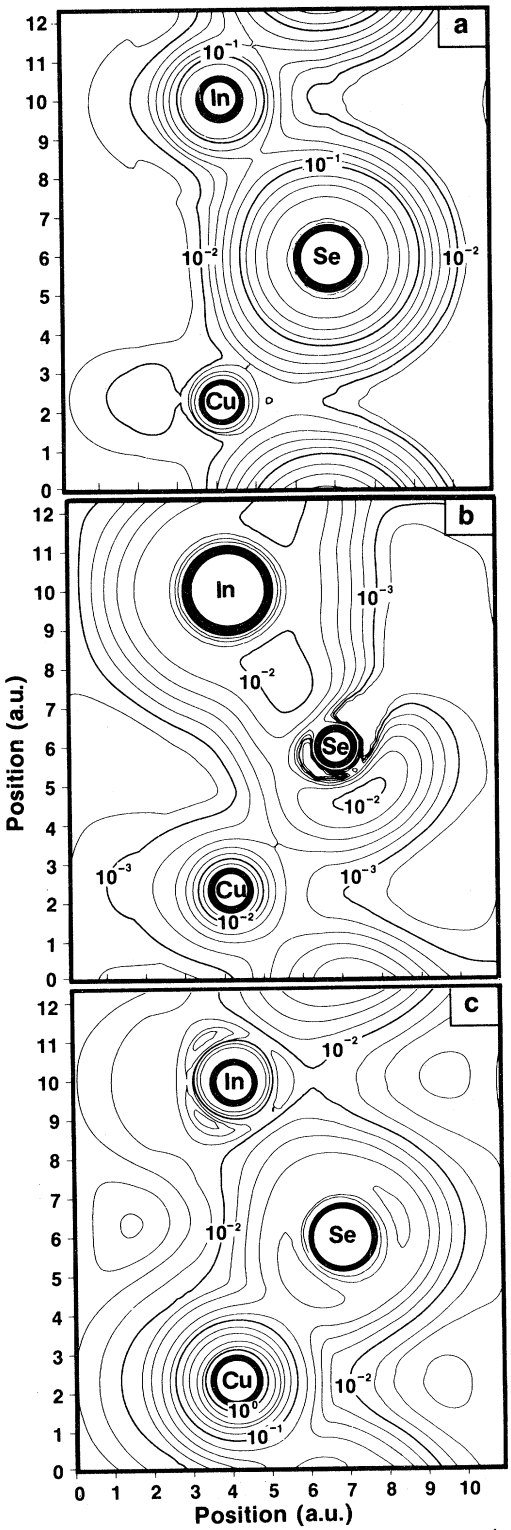

FIG. 9. Charge density for selected energy regions of the valence bands of $CuInSe_2$: Se $4s$ (-12 to -15 eV) in (a), In—Se bond (-5.5 to -6.5 eV) in (b), and the Cu $3d$—Se $4p$ bands (0. to -5.5 eV) in (c). The logarithmically spaced contours are described in the text. Solid rings indicate core regions.

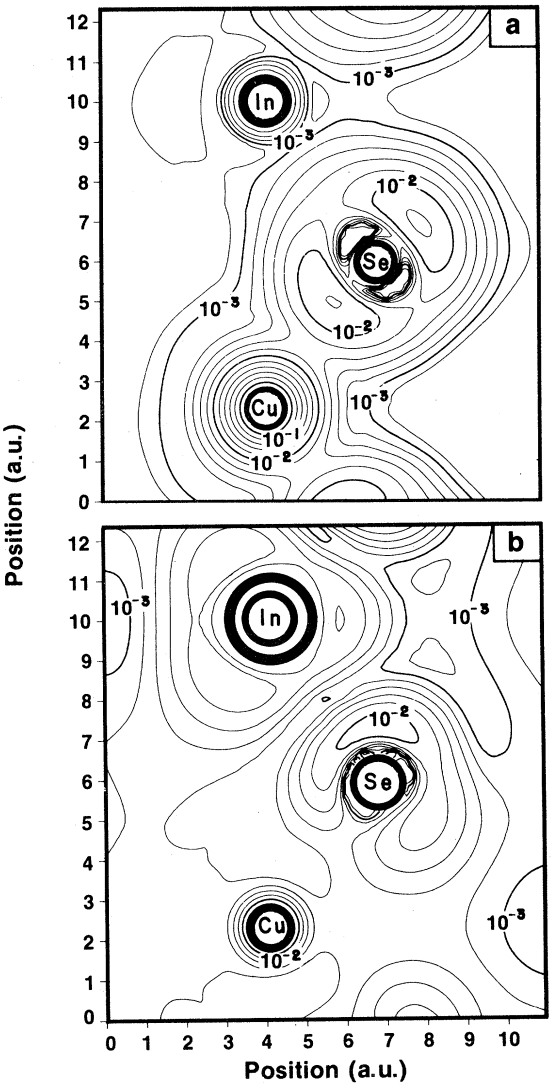

FIG. 10. Charge density of the optically active bands of $CuInSe_2$: (a) the top volt of the valence band and (b) the bottom volt of the conduction band. Contours are logarithmically spaced. Solid rings indicate core regions.

copy (XPS) results of Rife *et al.*[37] also shown in Fig. 7. Both experiment and theory place the In $4d$ and Se $4s$ levels near -17 and -13 eV, respectively. Since we neglect spin-orbit coupling, the In $4d$ appears as a single peak. Rife *et al.* observe a structure at -6.2 eV which they are unable to assign. Our charge densities show unambiguously that this is due to two bands forming a covalent bond between In $5s$ and Se $4p$. Next, XPS shows two peaks assigned as Cu $3d$ at -2.1 and -3.2 eV with a shoulder at -0.5 eV. We also assign states in this energy region to be dominant Cu $3d$, but the shape of the structure differs. We calculate a main peak at -4.2 eV with shoulders or perhaps lesser

TABLE VI. CuInSe band energies (in eV) at the symmetry points Γ and N with the use of Ceperley correlation and Slater xc. The zero of energy is set at the valence-band maximum.

	Γ		N (all doubly degenerate)	
Degeneracy	Ceperley	Slater	Ceperley	Slater
1	−14.00	−13.89	−13.18	−13.29
3	−12.75	−12.98	−12.96	−13.13
1	−6.32	−5.85	−6.17	−5.59
1	−5.52	−5.01	−5.02	−4.74
1	−4.66	−4.75	−4.31	−4.65
1	−4.53	−4.58	−4.08	−4.60
1	−4.49	−4.30	−3.73	−4.21
2	−4.22	−4.72	−3.73	−4.10
1	−3.93	−4.13	−3.21	−3.60
2	−3.85	−4.37	−2.65	−2.57
2	−3.52	−4.00	−1.52	−1.45
1	−3.38	−3.77	−0.99	−0.91
2	−3.22	−2.93	−0.63	−0.57
1	−2.72	−2.83	1.39	1.97
1	−2.48	−2.59	3.37	4.30
2	−2.32	−2.02	4.68	5.57
2	−0.03	−0.07	5.13	5.95
1	0.0	0.0		
1	0.03	0.73		
1	1.87	2.93		
1	2.46	3.09		
2	4.07	4.91		
1	4.63	5.54		
2	4.93	5.91		

TABLE VII. X-ray scattering amplitudes for $CuInSe_2$ in electrons per unit cell.

Beam	Amplitude	Beam	Amplitude
(0,0,0)	292.00	$(3,2,\frac{1}{2})$	14.62
$(0,0,\frac{1}{2})$	15.78	(3,1,2)	4.65
(1,1,1)	177.98	(3,0,2.5)	1.22
(1,0,1.5)	33.50	(3,2,1.5)	42.48
(2,0,0)	21.26	(4,0,0)	176.28
(0,0,2)	18.34	(0,0,4)	185.18
(2,0,1)	2.82	(4,0,1)	8.78
$(2,1,\frac{1}{2})$	36.08	(2,1,3.5)	29.31
(1,0,2.5)	30.36	$(4,1,\frac{1}{2})$	28.50
(2,3,1.5)	21.30	(3,7,3)	121.99
(2,2,0)	211.47	(3,3,1)	119.29
(2,0,2)	214.09	(3,2,2.5)	40.33
$(3,0,\frac{1}{2})$	44.11	(4,1,1.5)	35.70
(3,1,0)	4.98	(2,0,4)	12.92
(3,1,1)	139.70	(4,0,2)	19.19
(1,1,3)	142.81	(4,2,0)	21.36
(1,2,2.5)	19.88	(4,2,1)	6.19
(3,0,1.5)	1.45	(1,0,4.5)	11.64
(2,2,2)	19.66	(3,0,3.5)	37.18
(2,0,3)	2.40	(4,1,2.5)	34.07
(1,0,3.5)	12.61		

peaks at −3.0, −2.0, and −0.5 eV. The peak at −4.2 eV contains 60−70% Cu $3d$ admixed with Se $4p$. The $3d$ contribution decreases to about 30% at the top of the valence band. The presence of d-state character at and near the top of this band invalidates any calculation which does not explicitly include the d electrons.

Rife *et al.* observe from reflectivity measurements the leading edge of the conduction band near 1.4 eV. Next they observe two peaks at 2.9 and 3.4 eV. We are not able to distinguish these and instead calculate a single peak at 2.3 eV. This peak has In−Se antibonding character. Finally, we calculate two structures at 4.5 and 5.5 eV which have the same antibonding character.

The character of each of the above described peaks was deduced from local density of states (LDOS) and the charge density plots of Figs. 8−10. The contour plots show a plane containing three adjacent nuclei, one each of Cu, Se, and In. This plane is shown in Fig. 6. It does not correspond to any low-index plane because of the anion displacement—the fact that Cu−Se bonds are slightly shorter than In−Se bonds. Owing to the very large dynamic range of the densities, the con-

tours are at logarithmic intervals. Heavy contours are order-of-magnitude lines at $10^{-3}, 10^{-2}, 10^{-1}, 10^{0}$ electrons per cubic atomic unit. Figure 8(a) shows the total valence-band charge from all states in the interval -15 to 0 eV. Also shown in Figs. 8(b) and 8(c) are plots of the total charge density along the Cu—Se and In—Se bonds. These are also log plots. The panels of Fig. 9 show the three distinct energy regions of the valence band corresponding to the structures in the DOS: the Se $4s$ states (-12 to -15 eV), the In—Se bond (-5.5 to -6.5 eV), and the Cu $3d$—Se $4p$ mixed bands (0 to -5.5 eV). Finally Fig. 10 shows the charge distribution of the optically active bands—the top eV of the valence band and the bottom eV of the conduction band.

Figure 11 is the calculated band structure along the $T \rightarrow \Gamma \rightarrow N$ symmetry lines. The nature of bands in various energy regions is, of course, the same as described for the DOS. The one qualitatively incorrect feature is that we get a band gap of 0.0 ± 0.2 eV with Ceperley xc. This compares to experimental values of 1.00 ± 0.05 eV.[38–40] We interpret this discrepancy[30] as a failure of local-density theory, which is derived from the properties of a homogeneous electron gas, to adequately describe the highly localized $3d$ character of the valence bands. In general, one would expect the Coulomb self-interactions present in the local-density potential to push the $3d$ states to higher energy. This would raise the upper valence bands and reduce the principal gap. This hypothesis is consistent with the fact that we calculate the first distinct feature of the conduction-band DOS about an eV too close to the valence-band maximum. Another band calculation[41] of two ternary chalcopyrites also gets a gap drastically too small and the same large dispersion of the bottom conduction band. We also calculated the band gap with Slater xc ($\alpha = 1.0$). The resulting gap was about 0.7 eV, which is in much better agreement with experiment. The energy levels for Γ an N are given in Table VI for both Ceperley correlation and Slater xc. Finally, Table VII gives the x-ray scattering factors for the calculated $CuInSe_2$ charge density.

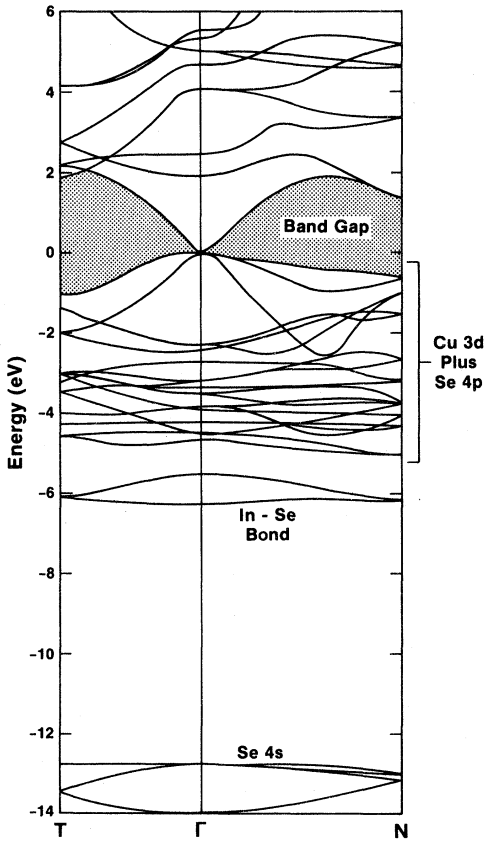

FIG. 11. Band structure of $CuInSe_2$ using Ceperley correlation.

APPENDIX A: VARIATION OF THE POTENTIAL

In our approach the independent variable is the potential $U_{\text{ext}}(\vec{r})$ or, more specifically, the potential parameters $\{\mu_p\}$. In order to carry out this approach we need the analytical derivatives of various quantities with respect to variation of μ_p. These formulas are developed here.

The potential is used to generate only independent-particle energies and wave functions; the resulting values are then used throughout the approach. The response of energies and wave functions to a change in the potential can be obtained by perturbation theory. For first derivatives it is sufficient to use first-order perturbation theory, which gives

$$\partial_p \epsilon_j = \langle \psi_j \mid \partial_p U_{\text{ext}} \mid \psi_j \rangle = \int d\vec{r}\, n_j(\vec{r})\partial_p U_{\text{ext}}(\vec{r}) , \tag{A1}$$

$$\partial_p \psi_j(\vec{r}) = \sum_{j' \neq j} \psi_{j'}(\vec{r}) \frac{1}{\epsilon_{j'} - \epsilon_j} \times \langle \psi_{j'} \mid \partial_p U_{\text{ext}} \mid \psi_j \rangle , \tag{A2}$$

where ∂_p denotes $\partial/\partial\mu_p$. The response of the charge density can be obtained as

$$\partial_p n(\vec{r}) = \sum_j \omega_j 2\,\mathrm{Re}[\psi_j^\dagger(\vec{r})\partial_p \psi_j(\vec{r})]$$
$$= \sum_j \omega_j \sum_{j' \neq j} \frac{2}{\epsilon_{j'} - \epsilon_j} \mathrm{Re}[\psi_j^\dagger(\vec{r})\psi_{j'}(\vec{r})\langle \psi_{j'} | \partial_p U_{\mathrm{ext}} | \psi_j \rangle] \,. \tag{A3}$$

Equation (2) is manipulated to obtain $-\frac{1}{2}\nabla^2\psi_j(\vec{r})$. This is inserted into Eq. (4), and the variation giving the change in kinetic energy is taken as

$$\partial_p T[n] = \sum_j \omega_j \left\{ \partial_p \epsilon_j - \int d\vec{r}\,[n_j(\vec{r})\partial_p U_{\mathrm{ext}}(\vec{r}) + U_{\mathrm{ext}}(\vec{r})\partial_p n_j(\vec{r})] \right\}$$
$$= -\int d\vec{r}\, U_{\mathrm{ext}}(\vec{r})\partial_p n_j(\vec{r}) \,. \tag{A4}$$

For the remaining terms of Eq. (1), the only term in the derivative comes from a change in $n(\vec{r})$, so the chain rule gives

$$\partial_p E_{\mathrm{tot}} = \int d\vec{r} \left[-U_{\mathrm{ext}}(\vec{r}) + V_{\mathrm{ext}}(\vec{r}) + \int d\vec{r}\,' \frac{n(\vec{r}\,')}{|\vec{r} - \vec{r}\,'|} + \frac{\partial E_{\mathrm{xc}}[n]}{\partial n(\vec{r})} \right] \partial_p n(\vec{r})$$
$$= \sum_j \omega_j \sum_{j' \neq j} \frac{2}{\epsilon_{j'} - \epsilon_j} \mathrm{Re}\{\langle \psi_j | V_{\mathrm{KS}} - U_{\mathrm{ext}} | \psi_{j'} \rangle \langle \psi_{j'} | \partial_p U_{\mathrm{ext}} | \psi_j \rangle\} \,, \tag{A5}$$

where V_{KS} is given by Eq. (8). A particularly interesting special case of this approach is obtained when V_{KS} can be fitted to the functional form $U_{\mathrm{ext}}(\vec{r}, \{\nu_q\})$, and this form is linear in each ν_q, so that

$$V_{\mathrm{KS}}(\vec{r}) - U_{\mathrm{ext}}(\vec{r}) = \sum_q (\nu_q - \mu_q)\partial_q U_{\mathrm{ext}}(\vec{r}) \,. \tag{A6}$$

Then

$$\partial_p E_{\mathrm{tot}} = \sum_q (\nu_q - \mu_q)\chi_{qp} \,, \tag{A7}$$

where

$$\chi_{qp} \equiv \sum_j \omega_j \sum_{j' \neq j} \frac{2}{\epsilon_{j'} - \epsilon_j} \mathrm{Re}\{\langle \psi_j | \partial_q U_{\mathrm{ext}} | \psi_{j'} \rangle \langle \psi_{j'} | \partial_p U_{\mathrm{ext}} | \psi_j \rangle\} \tag{A8}$$

is the generalized screened susceptibility. Clearly, the left-hand side of Eq. (A7) will vanish when ν_q equals μ_q, so this provides another derivation of the variational minimum condition Eq. (12).

The remaining derivative of interest is $\partial_p \nu_q$ since this forms the Jacobian matrix as

$$J_{qp} = \partial_p \nu_q - \delta_{pq} \tag{A9}$$

by taking the derivative of Eq. (13). The variations of the Coulomb and xc potentials are given by

$$\partial_p V_{\mathrm{Coul}}(\vec{r}) = \int d\vec{r}\,' \frac{1}{|\vec{r} - \vec{r}\,'|} \partial_p n(\vec{r}\,') \tag{A10}$$

and

$$\partial_p V_{\mathrm{xc}}(\vec{r}) = \frac{dv_{\mathrm{xc}}(n(\vec{r}))}{\partial n(\vec{r})} \partial_p n(\vec{r}) \,. \tag{A11}$$

The use of these to obtain the derivative of Eq. (31) gives

$$\partial_p v_q = \frac{1}{\Omega} \int d\vec{r}\, e^{-i\vec{G}_q \cdot \vec{r}} \left[\int d\vec{r}\,' \frac{1}{|\vec{r} - \vec{r}\,'|} \partial_p n(\vec{r}\,') + v_{\mathrm{xc}}'(n(\vec{r}))\partial_p n(\vec{r}) \right]$$
$$= \frac{1}{\Omega} \sum_j w_j \sum_{j' \neq j} \frac{2}{\epsilon_{j'} - \epsilon_j} \mathrm{Re}[\langle \psi_j | e^{-i\vec{G}_q \cdot \vec{r}} (\hat{J} + v_{\mathrm{xc}}') | \psi_{j'} \rangle \langle \psi_{j'} | \partial_p U_{\mathrm{ext}} | \psi_j \rangle] \,, \tag{A12}$$

where $\hat{J}$ is the Coulomb operator $1/|\vec{r}-\vec{r}'|$. This equation generally is not useful for evaluating $J_{qp}^{(m)}$ because it requires having all the eigenfunction $\psi_{j'}(\vec{r})$, and the double sum over double matrix elements is an N^4 process that usually is too expensive to be useful. However, the formula can be used as a guide for approximating $\underline{J}^{(m)}$, as we do for the quasi-Newtonian method.

APPENDIX B: MATRIX ELEMENTS IN THE MIXED BASIS REPRESENTATION

The following formulas are used for computing overlap and Hamiltonian matrix elements:

$$\langle \Phi_{\alpha nlm} | \Phi_{\alpha' n' l' m'} \rangle = \delta_{\alpha\alpha'}\delta_{nn'}\delta_{ll'}\delta_{mm'} \langle \Phi_{\alpha nlm} | \Phi_{\vec{G}} \rangle$$

$$= \frac{1}{\sqrt{\Omega}} i^l Y_{lm}^*(\vec{k}+\vec{G}) e^{i\vec{G}\cdot\vec{\tau}_\alpha} 4\pi \int_0^{r_{mc}} r^2 dr \frac{P_{nl}(r)}{r} j_l(r|\vec{k}+\vec{G}|) , \tag{B2}$$

$$\langle \Phi_{\vec{G}} | \Phi_{\vec{G}'} \rangle = \delta_{\vec{G}\vec{G}'} , \tag{B3}$$

$$\langle \Phi_{\alpha nlm} | \hat{H} | \Phi_{\alpha' n' l' m'} \rangle = \delta_{\alpha\alpha'} \left[\epsilon_{\alpha nlm} \delta_{nn'}\delta_{ll'}\delta_{mm'} + \sum_{l''m''} \left[\int_0^{r_{mc}} r\, dr \frac{P_{nl}(r)}{r} V_{\alpha l''m''}(r) \frac{P_{n'l'}(r)}{r} \right] \right.$$

$$\left. \times \left[\oint d^2\hat{r}\, Y_{lm}^*(\hat{r}) Y_{l''m''}(\hat{r}) Y_{l'm'}(\hat{r}) \right] \right] , \tag{B4}$$

$$\langle \Phi_{\alpha nlm} | \hat{H} | \Phi_{\vec{G}} \rangle = \epsilon_{\alpha nlm} \langle \Phi_{\alpha nlm} | \Phi_{\vec{G}} \rangle + \sum_p \mu_p \langle \Phi_{\alpha nlm} | \Phi_{\vec{G}+\vec{G}_p} \rangle , \tag{B5}$$

$$\langle \Phi_{\vec{G}} | \hat{H} | \Phi_{\vec{G}'} \rangle = \tfrac{1}{2} |\vec{G}|^2 \delta_{\vec{G}\vec{G}'} + \sum_\alpha v_\alpha(\vec{G}'-\vec{G}) + \mu_{\vec{G}'-\vec{G}} , \tag{B6}$$

where

$$V_{\alpha lm}(r) = 4\pi i^l \sum_p \mu_p e^{i\vec{G}_p\cdot\vec{\tau}_\alpha} j_l(G_p r) Y_{lm}^*(\hat{G}_p) , \tag{B7}$$

$$v_\alpha(\vec{G}) = \frac{4\pi}{\Omega} e^{-i\vec{G}\cdot\vec{\tau}_\alpha} \int_0^{r_{mc}} r^2 dr\, j_0(rG) v_\alpha(r) . \tag{B8}$$

These formulas are derived easily by using the spherical harmonic decomposition of a plane wave and the following facts: (i) Quasiatom spheres on different sites are nonintersecting, (ii) $\Phi_{\alpha nlm}(\vec{r})$ come from eigenfunctions of $-\frac{1}{2}\nabla^2 + v_\alpha(\vec{r})$, and (iii) all matrix elements are the integral over one unit cell due to the normalization chosen for basis functions. The last term of Eq. (B5) is the most expensive to compute, but can be evaluated for all $\vec{G}$ simultaneously by using FFT to perform the convolution sum.

For some very highly localized core basis functions a good approximation can be made in the Hamiltonian matrix elements. In these cases (see Sec. V A) the basis function can be assumed to be an eigenfunction of the final potential. One can then use

$$\langle \Phi_{\alpha nlm} | \hat{H} | \Phi \rangle = \epsilon_{\alpha nl} \langle \Phi_{\alpha nlm} | \Phi \rangle , \tag{B9}$$

where $\epsilon_{\alpha nl}$ is the energy expectation value obtained from Eq. (B4). In order that this approximation preserve the crystal symmetry of the Hamiltonian, one must neglect crystal-field splitting in the evaluation of $\epsilon_{\alpha nlm}$; i.e., the sum over l'',m'' in Eq. (B4) covers only the $l''=0$ term.

The first-order approximation for including the nonspherical multicentered terms into the xc potential is implemented as follows. First, one defines a density that excludes nonspherical terms as

$$\tilde{n}(\vec{r}) = n_{FS}(\vec{r}) + \sum_\alpha n_{\alpha 00}(|\vec{r}-\vec{\tau}_\alpha|) Y_{00}(\vec{r}-\vec{\tau}_\alpha) . \tag{B10}$$

This density contains the correct total number of electrons since the nonspherical multicentered terms integrate to zero and hence only redistribute

charge. The density $\tilde{n}(\vec{r})$ of Eq. (B10) is used to construct a $\tilde{V}_{xc}(\vec{r})$ by the methods of Sec. III D.

One now makes a Taylor-series expansion to include the nonspherical terms as

$$V_{xc}(\vec{r}) \cong v_{xc}(\tilde{n}(\vec{r})) + \sum_{\alpha} \sum_{l>0} \sum_{m} \frac{dv_{xc}(\tilde{n}(\vec{r}))}{d\tilde{n}(r)} n_{\alpha lm} \times (|\vec{r}-\vec{\tau}_{\alpha}|) Y_{lm}(\vec{r}-\vec{\tau}_{\alpha}) . \quad \text{(B11)}$$

The regions of space where the second term might contribute are in the core regions where $\tilde{n}(\vec{r})$ is dominated by the spherical core charge. Therefore, we make a second approximation that for computing the derivative of $v_{xc}(\tilde{n}(\vec{r}))$ in this region, it is sufficient to use a spherical symmetrization of $\tilde{n}(\vec{r})$, which is given by $n_{s\alpha}(\vec{r})$ from Eq. (29). Thus the first-order approximation is given by

$$V_{xc}(\vec{r}) = \tilde{V}_{xc}(\vec{r}) + \sum_{\alpha} \sum_{l>0} \sum_{m} \left[\frac{dv_{xc}(n_{s\alpha}(\vec{r}))}{dn_{s\alpha}(\vec{r})} n_{\alpha lm}(|\vec{r}-\vec{\tau}_{\alpha}|) \right] \times Y_{lm}(\vec{r}-\vec{\tau}_{\alpha}) . \quad \text{(B12)}$$

In this expression, the term in large parentheses depends only on the radial distance $|\vec{r}-\vec{\tau}_{\alpha}|$, so that the sum becomes the nonspherical multicentered contribution to $V_{xc}(\vec{r})$. The Fourier-series and spherical multicentered terms are in $\tilde{V}_{xc}(\vec{r})$ as described in Sec. III D.

[1]P. Hohenberg and W. Kohn, Phys. Rev. 136, B864 (1954).
[2]W. Kohn and L. J. Sham, Phys. Rev. 140, A1130 (1965).
[3]W. P. Wang, R. A. Parr, D. R. Murphy, and G. A. Henderson, Chem. Phys. Lett. 43, 409 (1976); J. A. Alonso and L. Girifalco, Phys. Rev. B 17, 3735 (1978).
[4]A. K. Theophilou, J. Phys. C 12, 5419 (1979).
[5]J. Catriel, J. Phys. C 13, L375 (1980).
[6]J. Catriel, Int. J. Quantum Chem. 19, 293 (1981).
[7]E. Feenberg, *Theory of Quantum Fluids* (Academic, New York, 1969); F. Y. Wu and E. Feenberg, Phys. Rev. 128, 943 (1962).
[8]J. W. Clark and P. Westhaus, Phys. Rev. 141, 833 (1966); M. L. Ristig and J. W. Clark, Nucl. Phys. A 199, 351 (1973).
[9]D. Ceperley, G. V. Chester, and M. H. Kalos, Phys. Rev. B 16, 3081 (1977).
[10]V. T. Rajan and C. W. Woo, Phys. Rev. B 18, 4048 (1978).
[11]Many applications exist for molecules; e.g., the CMO (correlated-molecular-orbital) method. See, for instance, A. A. Frost, J. Braunstein, and W. Schwemer, J. Am. Chem. Soc. 70, 3292 (1948); A. A. Frost and J. Braunstein, J. Chem. Phys. 19, 1133 (1951).
[12]R. Jastrow, Phys. Rev. 98, 1479 (1955); R. D. Murphy and R. O. Watts, J. Low Temp. Phys. 2, 507 (1970); B. Brandow, Phys. Lett. 61B, 117 (1976); H. A. Bruckner, Phys. Rev. C 14, 1999 (1976).
[13]J. A. Vergés and C. Tejedor, J. Phys. C 12, 499 (1979); W. Kohn, Phys. Rev. B 7, 4388 (1973).
[14]N. D. Lang and W. Kohn, Phys. Rev. B 1, 4555 (1970).
[15]For example, C. S. Wang and J. Callaway, Phys. Rev. B 15, 298 (1977); D. G. Laurent, C. S. Wang, and J. Callaway, *ibid.* 17, 455 (1978); J. E. Simmons, C. C. Lin, D. F. Fouquet, E. E. Lafon, and R. C. Chaney, J. Phys. C 8, 1549 (1975).
[16]M. L. Cohen, M. Schlüter, J. R. Chelikowsky, and S. G. Louie, Phys. Rev. B 12, 5575 (1975).
[17]G. W. Pratt, Phys. Rev. 88, 1217 (1952).
[18]L. G. Ferriera, J. Comput. Phys. 36, 198 (1980).
[19](a) M. Manninen, R. Nieminen, and P. Hautojavri, Phys. Rev. B 12, 4012 (1975); (b) G. P. Kerker, *ibid.* 23, 3082 (1981).
[20]J. H. Rose and H. B. Shore, Solid State Commun. 17, 327 (1975).
[21]J. H. Rose and H. B. Shore, Phys. Rev. B 17, 1884 (1978).
[22]J. N. Bass, A. E. S. Green, and J. H. Wood, Adv. Quantum Chem. 7, 263 (1973); R. H. Garvey, C. H. Jackman, and A. E. S. Green, Phys. Rev. A 12, 1144 (1975).
[23]A. Aashamar, T. M. Luke, and J. C. Talman, Phys. Rev. A 19, 6 (1979); J. D. Talman and W. F. Shadwick, *ibid.* 14, 36 (1976).
[24]J. E. Dennis, Jr. and Jorge J. Moré, SIAM (Soc. Ind. Appl. Math.) Review 19, 46 (1977); C. G. Broyden, Math. Comput. 19, 577 (1965).
[25]A. Zunger and A. J. Freeman, Int. J. Quantum Chem. S 10, 383 (1976); Phys. Rev. B 15, 4716 (1977).
[26]J. W. Cooley and J. W. Tukey, Math. Comput. 19, 297 (1965).
[27]C. D. Gelatt, Jr., H. Ehrenreich, and R. E. Watson, Phys. Rev. B 15, 1613 (1977).
[28]R. N. Euwema, D. J. Stukel, and T. C. Collins, in *Computational Methods of Band Theory,* edited by P. M. Marcus, J. F. Janak, and A. R. Williams (Plenum, New York, 1971), p. 82.
[29]D. M. Ceperley and B. J. Alder, Phys. Rev. Lett. 45, 566 (1980); D. M. Ceperley, Phys. Rev. B 18, 3126

(1978).
[30]J. P. Perdew and A. Zunger, Phys. Rev. B 23, 5048 (1981).
[31]P. Puley, Chem. Phys. Lett. 73, 393 (1980).
[32]For example, see W. A. Harrison, *Electron Structure* (Freeman, San Francisco, 1980), p. 377.
[33]D. R. Hamann, Phys. Rev. Lett. 42, 662 (1979).
[34]C. S. Wang and B. M. Klein, Phys. Rev. B 24, 3393 (1981).
[35](a) S. Wagner, J. L. Shay, P. Miglicrata, and H. M. Kasper, Appl. Phys. Lett. 25, 434 (1974); (b) J. L. Shay, S. Wagner, K. Bachmann, E. Buehler, and H. M. Kasper, *Proceedings of the 11th IEEE Photovoltaics Specialties Conference* (IEEE, New York, 1975), p. 503; (c) L. L. Kazmerski, M. S. Ayyagari, and G. A. Sanborn, J. Appl. Phys. 46, 4685 (1975).
[36]R. A. Mickelsen and W. S. Chen, *Proceedings of the Fifteenth IEEE Photovoltaic Specialties Conference—1981* (IEEE, New York, 1981), p. 880.
[37]J. C. Rife, R. N. Dexter, P. M. Bridenbaugh, and B. W. Veal, Phys. Rev. B 16, 4491 (1977).
[38]C. Rincón, J. Gonzáles, and G. S. Parez, Phys. Status Solidi 108, K19 (1981).
[39]I. V. Bodnar, B. V. Korsun, and A. I. Lukomski, Phys. Status Solidi 105, K143 (1981).
[40]W. Hörig, H. Neumann, H. Sobotta, B. Schumann, and G. Kühn, Thin Solid Films 48, 67 (1978).
[41]T. Oguchi, T. Hamajima, T. Kambara, and K. I. Gondaira, Jpn. J. Appl. Phys. 19, 107 (1980).